PERGAMON

Journal of Asian Earth Sciences 19 (2001) 429–451

Journal of Asian Earth Sciences

www.elsevier.nl/locate/jseaes

Palaeomagnetic investigation in the Pamirs and its tectonic implications

M. Waldhör, E. Appel, W. Frisch, A. Patzelt

Institut für Geologie u. Paläontologie, Universität Tübingen, Sigwartstr. 10, 72076 Tübingen, Germany

Accepted 5 May 2000

Abstract

This paper presents a palaeomagnetic investigation in the Pamirs of Tadjikistan. Remanences are mainly carried by magnetite and are of secondary, synfolding origin. Application of a new method, the *small-circle reconstruction*, allows to extract palaeomagnetic rotation and tectonic tilting since the time of remanence acquisition (assumed to be ~20 Ma). In some regions consistent rotations are observed: (i) clockwise in the Muzkol area of the central Pamirs; (ii) following the trend of oroclinal bending in the northern Pamirs; and (iii) counterclockwise in the northern folded sequence of the southern Pamirs. However, variations within different regions are obvious and scattering even occurs within smaller areas. Most likely, local block rotations are caused by N–S shortening.

Palaeomagnetic and tectonic results reveal that tilt axes are rotated around vertical axes in the course of progressive shortening/folding. Surprisingly, the scatter of the tilt axes is reduced hereby. By comparing the distributions of the present and former tilt axes the amount of shortening is estimated for the southern Pamirs (shortened to ~40%) and the central Pamirs (shortened to ~60%).

Keywords: Palaeomagnetic investigation; Pamirs, Tadjikistan; Tectonic interpretation

1. Geological setting and drift history of the pamirs

This paper focuses on the tectonic interpretation of new palaeomagnetic data obtained from the Pamir region of Tadjikistan. The Pamir mountains are part of the northwestern edge of the India–Asia collision zone. A detailed review of the geology and tectonics is given by Burtman and Molnar (1993). Only aspects relevant to our work will be discussed here.

On the basis of the Palaeozoic and Mesozoic sutures, the Pamir area is divided into a northern, central and southern zone (Fig. 1). The northern and central Pamirs are considered to be part of Eurasia since the Late Palaeozoic, and the southern Pamirs since the Early Cretaceous.

The northern Pamirs mainly consists of Late Triassic to Early Jurassic granites and Palaeozoic metamorphic rocks. At the northern rim, folded and northward thrusted Cretaceous limestones and red beds, as well as Tertiary sandstones and red beds occur.

The northern part of the central Pamirs comprises an intensely folded sequence of Palaeozoic, Mesozoic and Tertiary sedimentary rocks. The boundary between the central and the southern Pamirs is delineated by a dome of high-grade metamorphic rocks, which have Ar–Ar and fission track cooling ages of ~20 Ma (Schwab et al., 1999). On both sides of the metamorphic dome, the rocks underwent intense folding and metamorphism with increasing grade towards the dome.

The southern Pamirs comprises Carboniferous to Permian sandstones and Triassic to Jurassic limestones in their eastern part. Apatites from intruded granites give fission track ages of ~20 Ma. Tertiary sandstones and red beds crop out along the southern boundary of the metamorphic dome. The cooling age of ~20 Ma, assigned to the rocks of the southern and central Pamirs, indicate a major thermotectonic event in the investigated area.

Taking into consideration the northward displacement of the sutures, the fault displacements and the balanced cross sections, a total convergence of 300-700 km is supposed to have occurred from the southern Pamirs to the Alai range (Burtman and Molnar, 1993). The available palaeomagnetic declination data from the surrounding areas seem to indicate the overall oroclinal bending around the western syntaxis (see Fig. 1).

Expected palaeofield declinations and inclinations for a reference location (southern Pamirs), now at a longitude/latitude 74.00°E/38.00°N, are shown in Fig. 2 for the period since Jurassic. These values will be taken as reference directions.

E-mail address: erwin.appel@uni-tuebingen.de (E. Appel).

1367-9120/01/$ - see front matter
PII: S1367-9120(00)00030-4

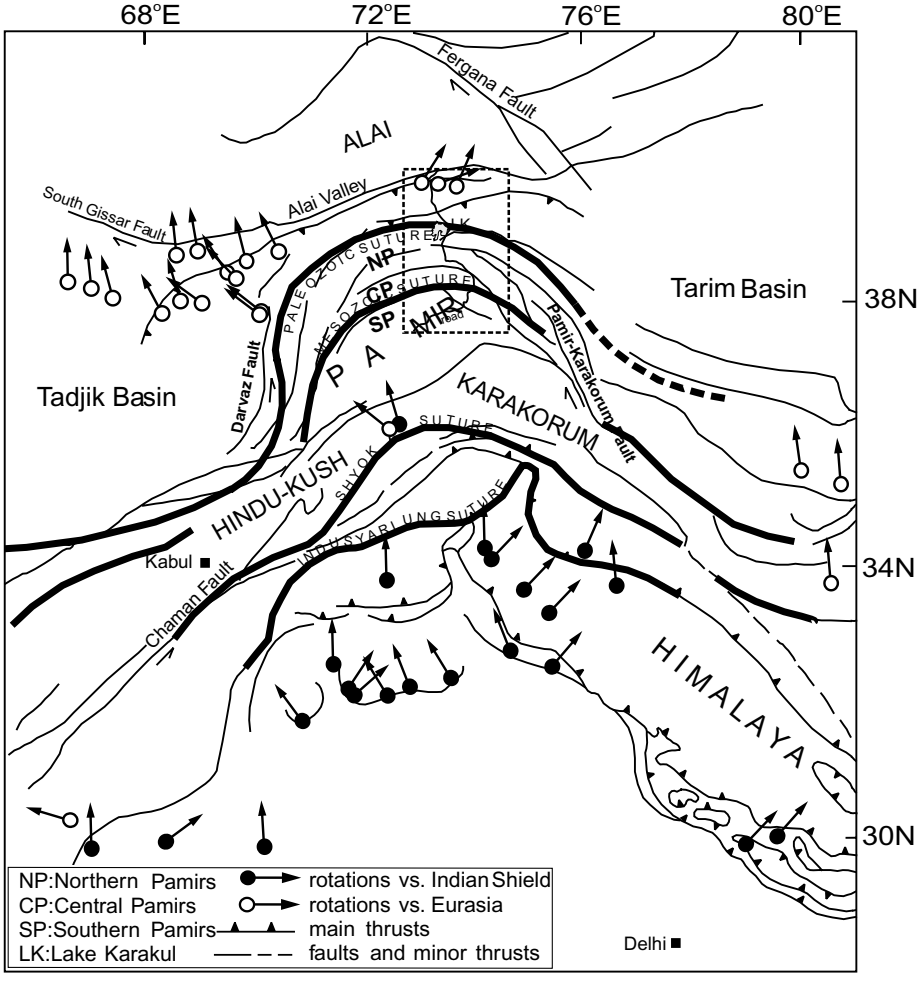

Fig. 1. Regional tectonic map of south-central Asia, showing sutures and major faults. The area of investigation is marked by the dashed rectangle in the north-western part of the India–Asia collision zone (NP, CP, SP denote the northern, central, southern Pamirs). Palaeomagnetic rotations in and around the western syntaxis are marked by arrows (modified from Klootwijk et al., 1986, 1991, 1994; Burtman and Molnar, 1993; Thomas et al., 1994 and Patzelt et al., 1996).

2. The small circle reconstruction

2.1. The principle

In this paper a small-circle reconstruction is used for processing palaeomagnetic remanence directions. A brief summary will be given below. The method is described in detail by Waldhör (1999).

The reconstruction essentially consists of three steps:

1. The corresponding palaeofield inclination (reference field) at the time of remanence acquisition is estimated from the APWP or from the in-situ remanence directions.
2. The in-situ remanences are rotated back to the reference field, thus determining angles of block rotation and tectonic tilting.
3. The remanence character is assessed from the amount of backtilting (primary remanences are identified by ~100% backtilting). Conventional fold tests do not play a prominent role in the small circle reconstruction but may be additionally applied.

The basic idea is as follows: through tilting, the in-situ remanence directions rotate on a small circle (*remanence small circle*) which is perpendicular to the tilt axis (Fig. 3). For different tilt angles within a folded sequence or for synorogenic remanence acquisition, the remanence directions will be distributed around a mean small-circle. The position of such a remanence small circle depends on the field direction during remanence acquisition and the trend of the tilt axis. The angular distance d (Fig. 3a and b) of a remanence small-circle in respect to the great circle of the tilting direction is given by:

$$d = \cos t \cos I_{\mathrm{acq}} \tag{1}$$

In this equation, t is the trend of the original tilt axis ($0° \leq t < 180°$), I_{acq} is the inclination of the acquisition field, and d is given as a fraction of the radius ($r = 1$) of the sphere.

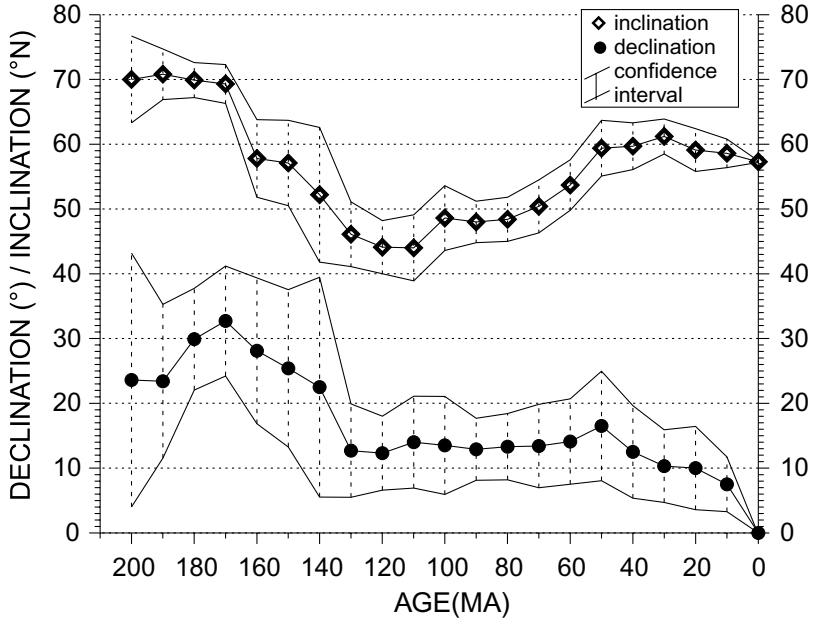

Fig. 2. Expected declinations and inclinations from the Jurassic to present for a reference location now at 74.0°E/38.0°N longitude/latitude (using the Eurasian APWP for stable Eurasia of Besse and Courtillot, 1991). A95 is used as the confidence interval for the inclination. For the declination, the approximation $A_{95}/\cos I$ is used instead of the true asymmetric confidence interval. Declinations (palaeomagnetic rotations) are all clockwise; inclinations are related to a position on the northern hemisphere.

When I_{acq} is known, the trend of the original tilt axis can be calculated from the angular distance d. The block rotation can be determined by comparing the calculated tilt axis with the observed one. The small circle reconstruction uses the same assumptions as usual, i.e. horizontal tilt axes and block rotation around vertical axes.

For a given in-situ remanence direction with D/I (declination/inclination), the angular distance d in respect to the corresponding tilting direction is calculated:

$$d = \cos(D - t^*) \cos I \tag{2}$$

Here t^* is the trend of the present (observed) tilt axis.

From this two different trends of the (original) tilt axis, $t1'$ *and* $t2'$, result:

$$t'_1 = \text{arc cos}(+d/\cos I_{acq}) + D_{acq} \tag{3a}$$

$$t'_2 = \text{arc cos}(-d/\cos I_{acq}) + D_{acq} \text{ or} \tag{3b}$$

$$t'_2 = 180° - t'_1 + 2D_{acq} \tag{3c}$$

Here D_{acq}, I_{acq} denote the normal polarity reference field (field of remanence acquisition).

Dacq can be assumed to be zero. The required palaeoinclination I_{acq} can be obtained directly from the assumed E–W tilted sites (original trend; Fig. 3b), where:

$$I_{acq} = \text{arc cos } |d| \tag{4}$$

Another approach to determine I_{acq} will be shown later (see Fig. 9).

Each of the two reconstructed original tilt axes is rotated around a vertical axis to match the present tilt axis. The rotation is either in the direction towards the normal polarity reference field, or in the opposite sense towards the reverse reference field. Thus, there are always four alternative reconstructions for tilting and block rotations $<180°$. The likelihood of the different possibilities have to be assessed by other criteria than magnetic ones, e.g. using information from nearby sites and bedding (i.e. upright/overturned).

The small-circle reconstruction can be applied to real small-circle distributions (either using several sites in a unidirectionally folded sequence, or single sites with asynchronous and synorogenic remanence acquisition) as well as to Fisher site means. Using Fisher means (as mostly done in this paper), angles of backtilting can be calculated and the remanence character (primary, secondary, synorogenic) can be assessed; statistical parameters k and α_{95} are as usual. For real small-circle distributions (e.g. in Fig. 8) a full statistical treatment of confidence limits is not yet available.

2.2. Example for small circle reconstruction

For a better understanding, the small circle reconstruction is demonstrated for one site (site 22) from the Pamir data set (Fig. 4). Site mean directions are used to calculate angles of backtilting and block rotations (as usually done in this paper). Conventions are as defined in Fig. 3.

A remanence small circle (running through the site mean direction) is defined parallel to the great circle of the present (observed) tilting direction. In the first step of our

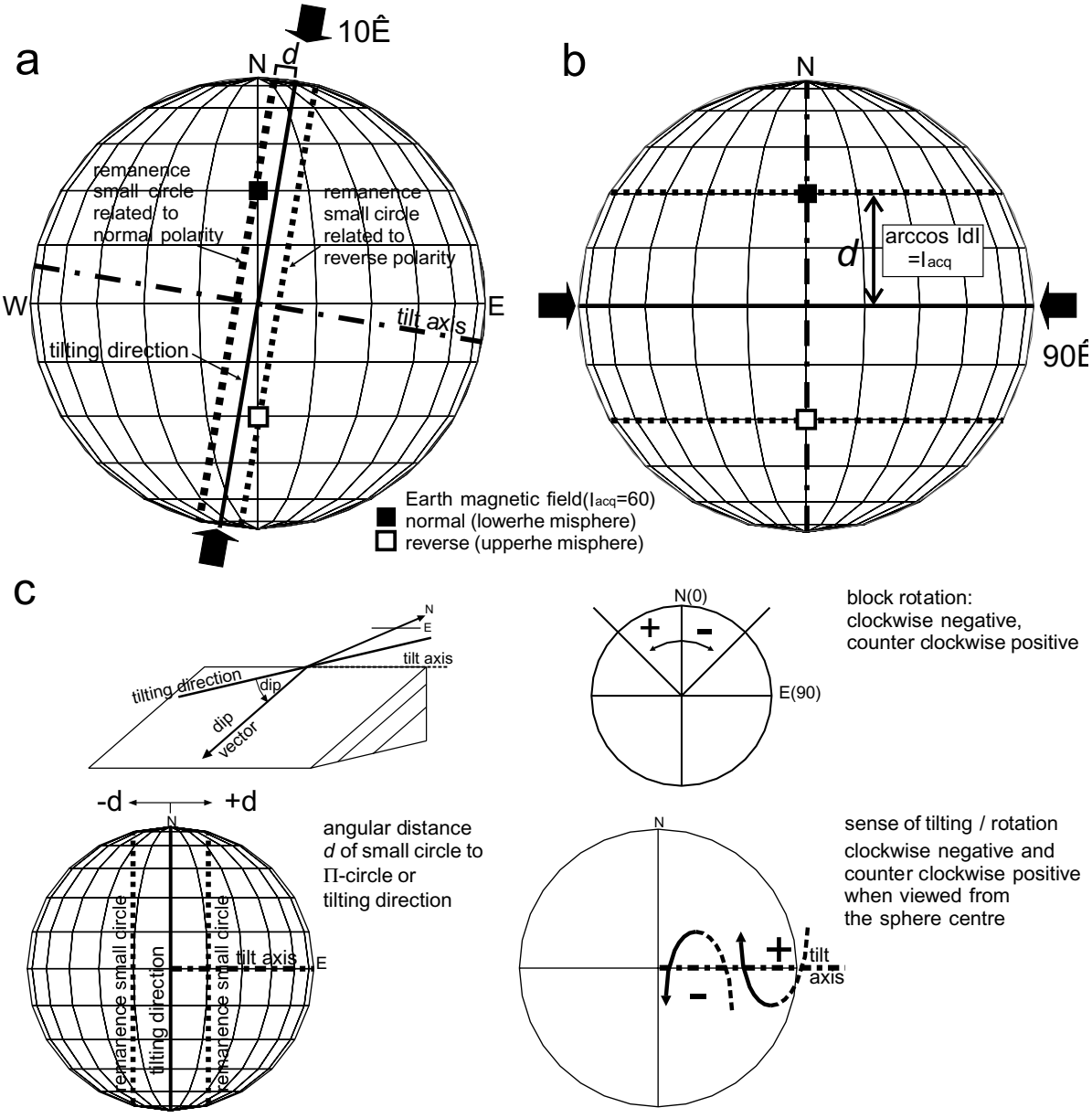

Fig. 3. Principle relationship between folding and remanence directions. Through tilting (folding) remanence directions rotate on small circles. The angular distance d is dependent on the tilt direction. (a) Tilt direction of 10° (fold axis horizontal); the remanence acquisition field is chosen as $D/I_{acq} = 0°/60°$ here; one small circle is related to normal polarity (closed square), the other one to reverse polarity (open square). Orthographic projection is chosen in this figure. (b) Same as in (a), but with a 90° oriented tilting. (c) Conventions used in this paper. See text for further explanations.

reconstruction the site mean direction is moved along the remanence small circle to the intersection point with the small circle of constant inclination. The corresponding angle of displacement on the remanence small circle represents the angle of backtilting (bt). Then, in a second step, the site mean direction is further moved along the small circle of constant inclination until it matches the reference (acquisition) field (here $D/I = 0°/55°$). This rotation denotes the angle of block rotation (br). Four alternative reconstructions with br and $bt < 180°$ exist and are shown in Fig. 4b–e. Reconstructions I/II and III/IV refer to normal and reverse polarity acquisition field, respectively.

Reconstruction I (Fig. 4b) yields a minor backtilting of $bt = -2°(-4\%)$ and moderate clockwise block rotation ($br = -69°$). In this interpretation, the remanence was acquired after tilting and the magnetic record involves mainly a block rotation since the age of remanence acquisition. As reconstruction I requires the smallest total rotation it can be considered as the most probable solution. For site 22 this selection by probability is quite clear as the alternative reconstructions II, III, and IV (Fig. 4c–e) require

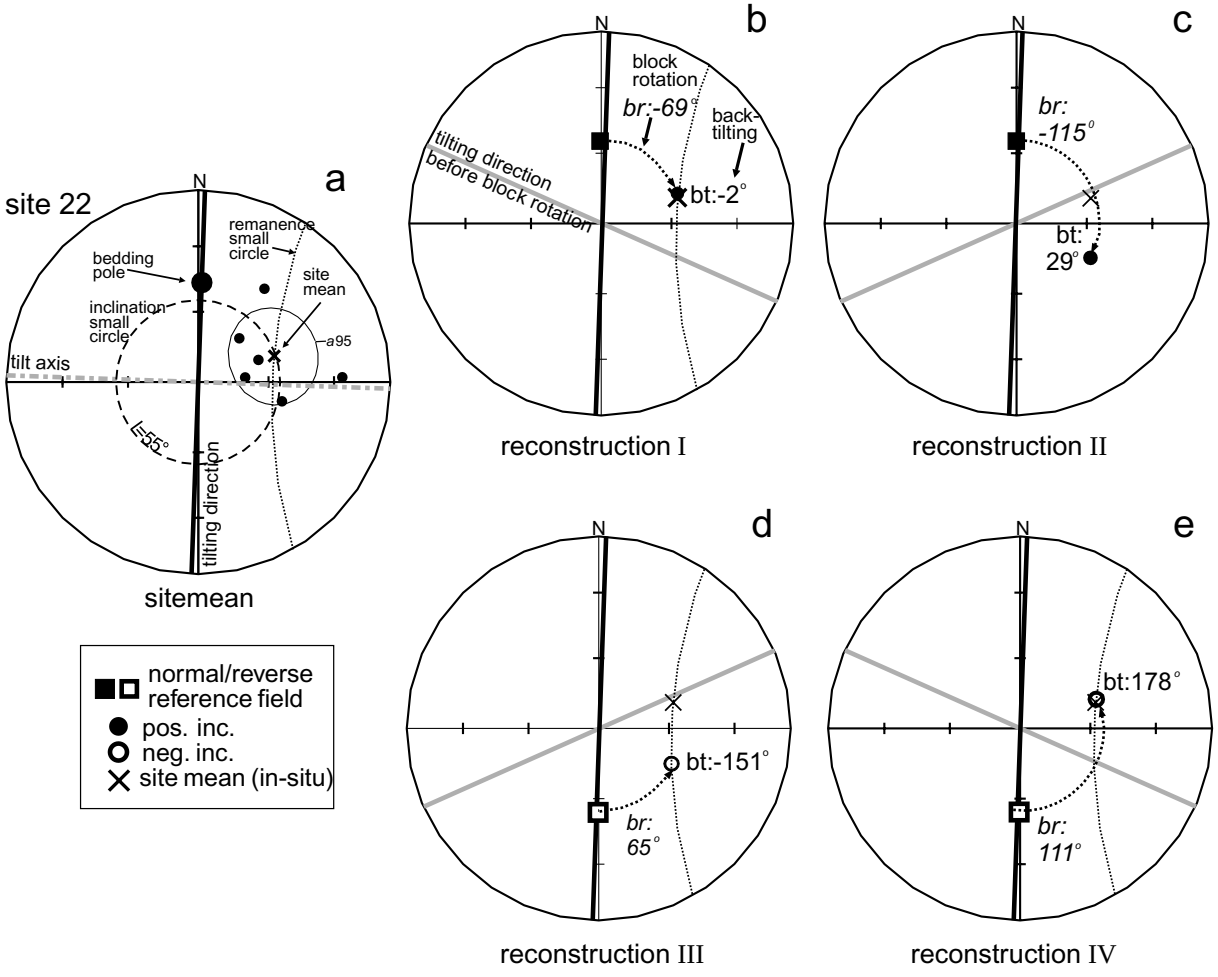

Fig. 4. The four alternative small circle reconstructions for site 22. The reference (acquisition) field is at $D/I = 0°/55°$ (normal polarity) and reverse, defining a small circle of constant inclination (here $I = 55°$; dashed line). The remanence small circle (dotted line) is fixed by the site mean direction parallel to the great circle (thick black line) of the observed tilting direction. Open/full circles in (b)–(e) show the site mean direction after backtilting along the remanence small circle to the intersection with the small circle of constant inclination. The thick grey line is the original tilting direction (after restoring block rotation). Conventions are as defined in Fig. 3. Stereographic projection is chosen in this figure. For further explanation see text.

much larger rotation angles of bt = 29°(67%) and br = −115°, bt = −151°(−351%) and br = 65°, bt = 178°(415%) and br = 111°, respectively. Also notice that the measured bedding dip (43°) does not allow to reach the reconstructed positions within the range of backtilting for an upright bedding dip of 43° and an overturned bedding dip of 137°. Hence, only tilting by more than 180° or two-phase tilting with opposite sense can explain the solutions II, III, and IV.

Not all investigated sites allow such a clear and reliable decision according to likelihood as site 22. Because of ambiguities, some erroneous directions may survive in the final data set. However, with the large number of sites available, they will not severely mislead the general interpretation. It also has to be emphasised, that without the small circle reconstruction our palaeomagnetic data from the Pamirs could not be interpreted as conventional techniques fail in case of a synorogenic remanence acquisition.

3. Sampling and laboratory procedure

Sampling in the field was done with a portable drill and a magnetic compass was used for orientation. Site locations are shown in Fig. 5. Exact positions were determined by GPS measurements. In Table 1 locations, lithologies and geological ages of all analysed sites are listed.

Rockmagnetic investigations were made on selected specimens, involving isothermal remanence acquisition (IRM; using a CRYOGENIC superconducting magnet to generate IRM up to 4.5 T, and a MOLSPIN spinner magnetometer to measure IRM), subsequent thermal

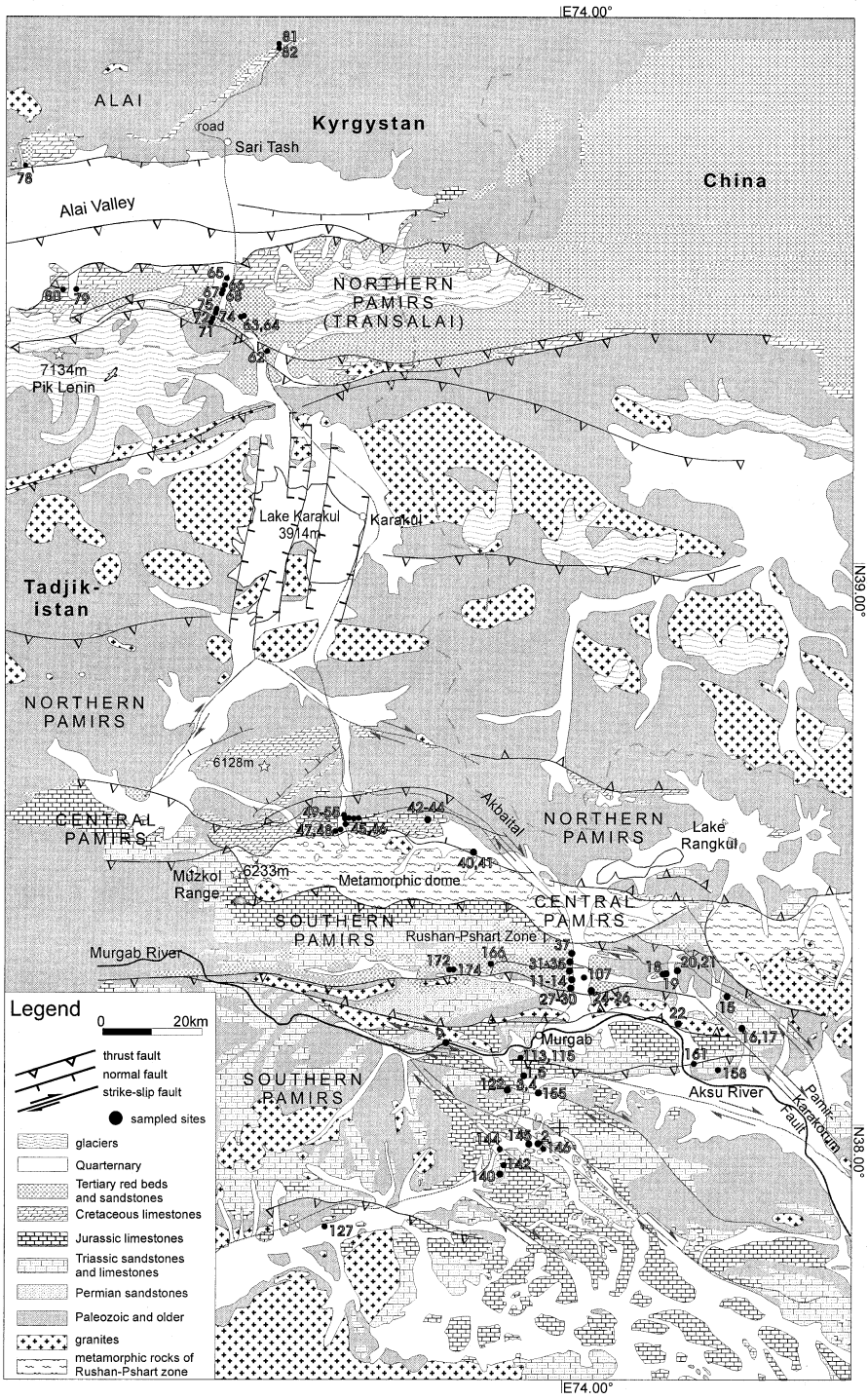

Fig. 5. Geological map of the investigation area with palaeomagnetic sampling sites. Modified from the geological maps (1:500,000) of the Russian Geology Ministry (1980, 1984) and from the maps of Strecker et al. (1995).

demagnetisation of a saturation IRM (SIRM), and Curie temperature determination by thermomagnetic runs of susceptibility (using an AGICO KLY-2 kappabridge with an attached CS-2 heating unit). For thermal (TH) and alternating (AF) demagnetisation a MAGNETIC MEASUREMENTS MMTD1 furnace and a 2G ENTERPRISES degausser were used, respectively. Palaeomagnetic remanence measurements were done with a RF-SQUID magnetometer including an automatic AF-degausser (2G ENTERPRISES). Remanence directions were determined by principal component analysis (PCA, modified version after Kirschvink, 1980). Fisher

Table 1
Location, lithology and geological ages of the analysed sites. Lithology and ages are taken from the geological maps (1:500,000) of the Russian Geology Ministry (1980, 1984). Tertiary sediments cannot be subdivided (as ages given in the Russian maps have to be considered as uncertain). Numerical ages are according to the time table from Ogg (1995). demag.: demagnetisation (AF: alternating field, TH: thermal). The right column indicates whether a significant site mean ($k \geq 10$) could be obtained.

Site	Location		Lithology	Geological age	Num. age (Ma)	Demag.	$k \geq 10$
	Lat.	Long.					Yes/no
Southern Pamirs							
1	38.09	73.90	Sandstone	Early Permian	290–256	TH	Yes
2	37.96	73.96	Limestone	Early to Middle jurassic	208–157	AF	Yes
3	38.11	73.91	Limestone	Early to Middle jurassic	208–157	AF	Yes
4	38.11	73.91	Limestone	Early to Middle Jurassic	208–157	AF	Yes
5	38.10	73.90	Sandstone	Early Permian	290–256	AF	Yes
6	38.10	73.90	Sandstone	Early Permian	290–256	TH	Yes
9	38.14	73.74	Sandstone	Early Permian	290–256	TH	Yes
11	38.27	74.04	Red beds	Tertiary	65–2	TH	No
12	38.27	74.04	Red beds	Tertiary	65–2	TH	No
13	38.27	74.04	Red beds	Tertiary	65–2	TH	Yes
14	38.27	74.05	Red beds	Tertiary	65–2	TH	Yes
15	38.23	74.37	Red beds	Tertiary	65–2	TH	Yes
16	38.16	74.41	Red beds	Tertiary	65–2	TH	Yes
17	38.16	74.41	Red beds	Tertiary	65–2	TH	Yes
18	38.27	74.25	Sandstone	Tertiary	65–2	AF	Yes
19	38.27	74.25	Sandstone	Tertiary	65–2	AF	Yes
20	38.27	74.27	Red beds	Tertiary	65–2	TH	No
21	38.27	74.27	Red beds	Tertiary	65–2	TH	No
22	38.16	74.29	Limestone	Early to Middle Jurassic	208–157	AF	Yes
24	38.25	74.06	Red beds	Tertiary	65–2	TH	Yes
25	38.25	74.06	Red beds	Tertiary	65–2	TH	Yes
27	38.25	74.05	Red beds	Tertiary	65–2	TH	Yes
29	38.26	74.05	Red beds	Tertiary	65–2	TH	Yes
30	38.26	74.05	Red beds	Tertiary	65–2	TH	Yes
31	38.28	74.08	Sandstone	Tertiary	65–2	TH	Yes
32	38.27	70.04	Red beds	Tertiary	65–2	TH	No
33	38.27	70.04	Sandstone	Tertiary	65–2	AF	No
34	38.31	70.04	Sandstone	Tertiary	65–2	TH	Yes
35	38.31	70.04	Sandstone	Tertiary	65–2	TH	Yes
37	38.31	70.04	Sandstone	Tertiary	65–2	AF	Yes
107	38.26	70.06	Red beds	Tertiary	65–2	TH	Yes
113	38.12	70.06	Limestone	Middle Jurrasic	178–157	AF	Yes
115	38.11	73.91	Limestone	Early to Middle jurassic	208–157	AF	Yes
122	38.06	73.88	Limestone	Early to Middle Jurassic	208–157	AF	Yes
127	37.82	73.47	Limestone	Middle Jurassic	178–157	AF	Yes
140	37.91	73.87	Limestone	Early to Middle Jurassic	208–157	AF	Yes
142	37.93	73.88	Limestone	Early Jurassic	208–178	AF	Yes
144	37.96	73.87	Limestone	Early jurassic	208–178	AF	Yes
145	37.97	73.93	Limestone	Early to Middle Jurassic	208–157	AF	Yes
146	37.96	73.97	Limestone	Early to Middle Jurassic	208–157	AF	Yes
155	38.06	73.95	Limestone	Early to Middle Jurassic	208–157	AF	Yes
158	38.10	74.36	Sandstone	Early Permian	290–256	AF	Yes
161	38.11	74.31	Sandstone	Early Permian	290–256	AF	Yes
166	38.29	73.84	Red beds	Late Cretaceous	97–65	TH	No
172	38.28	73.75	Red beds	Late Cretaceous	97–65	TH	No
174	38.27	73.76	Red beds	Late Cretaceous	97–65	TH	No
Central Pamirs							
40	38.47	73.81	Red beds	Tertiary	65–2	TH	Yes
41	38.48	73.81	Red beds	Tertiary	65–2	TH	Yes
42	38.54	73.73	Limestone	Late Cret.	97–65	AF	Yes
43	38.54	73.73	Limestone	Late Cret.	97–65	AF	Yes
44	38.54	73.73	Limestone	Late Cret.	97–65	AF	Yes
45	38.53	73.53	Red beds	Tertiary	97–65	TH	Yes
46	38.53	73.53	Red beds	Tertiary	97–65	TH	Yes
47	38.53	73.52	Red beds	Tertiary	65–2	TH	Yes
48	38.53	73.51	Red beds	Tertiary	65–2	TH	Yes

Table 1 (*continued*)

Site	Location		Lithology	Geological age	Num. age (Ma)	Demag.	$k \geq 10$
49	38.53	73.53	Limestone	Middle to Late Jurassic	178–146	AF	Yes
50	38.53	73.53	Limestone	Middle to Late Jurassic	178–146	AF	Yes
51	38.53	73.53	Limestone	Middle to Late Jurassic	178–146	AF	Yes
52	38.53	73.54	Limestone	Middle to Late Jurassic	178–146	AF	Yes
53	38.53	73.55	Limestone	Middle to late jurassic	178–146	AF	Yes
54	38.54	73.53	Limestone	Middle to late jurassic	178–146	AF	Yes
55	38.54	73.53	Limestone	Middle to Late Jurassic	178–146	AF	Yes
Northern Pamirs							
62	39.38	73.33	Sandstone	Tertiary	65–2	TH	Yes
63	39.41	73.27	Red beds	Tertiary	65–2	TH	No
64	39.41	73.27	Red beds	Tertiary	65–2	TH	Yes
65	39.50	73.24	Limestone	Early Cretaceous	146–97	AF	Yes
66	39.49	73.22	Red beds	Late Cretaceous	97–65	TH	Yes
67	39.48	73.23	Limestone	Early Cretaceous	97–65	AF	Yes
68	39.48	73.22	Red beds	Late Cretaceous	97–65	TH	Yes
71	39.43	73.20	Red beds	Tertiary	65–2	TH	Yes
72	39.43	73.21	Red beds	Tertiary	65–2	TH	No
74	39.44	73.21	Limestone	Early Cretaceous	146–97	AF	Yes
78	39.71	72.78	Red beds	Tertiary	65–2	TH	Yes
79	39.48	72.89	Red beds	Late Cretaceous	97–65	TH	Yes
80	39.48	72.86	Red beds	Late Cretaceous	97–65	AF	No
81	39.92	73.35	Sandstone	Tertiary	65–2	AF	No
82	39.92	73.35	Sandstone	Tertiary	65–2	TH	Yes

statistics were used for calculating site mean directions (Fisher, 1953).

4. Rock- and palaeomagnetic measurements, results and fold tests

4.1. Magnetic mineralogy

Fig. 6 shows examples of isothermal remanence (IRM) acquisition, thermal demagnetisation of a saturation IRM (SIRM) and demagnetisation of the natural remanence (NRM). The rock and palaeomagnetic results are listed in Table 2 (only sites with $k \geq 10$).

According to coercivities (shown by the saturation fields during IRM acquisition and alternating field demagnetisation of NRM) and unblocking temperatures (shown by thermal demagnetisation of NRM and SIRM) the magnetic remanences are predominantly carried by magnetite. Hematite is also encountered together with magnetite, mainly in the sandstones and red beds. Goethite contribution is of minor importance.

4.2. 4.2 Remanence analysis

Table 2 shows the details of demagnetisation (AF or TH) and component analysis (in situ and bedding corrected remanence directions). The demagnetisation behaviour is mostly clear and remanence components can be easily extracted with PCA. Separation of the contribution of hematite is not attempted because a significant contribution is only available in few specimens. From totally 77 analysed sites, 64 yield significant site mean directions ($k \geq 10$ for in situ remanences). In all 7 sites from the Middle to Late Jurassic limestones of the central Pamirs and in 6 other sites two well defined remanence components ($k \geq 10$), a low and a high coercive one, occur.

Permian sandstones of the southern Pamirs (sP) show a stable magnetite remanence, isolated by TH (sites 1,6,9) as well as AF (sites 5,158,161) demagnetisation. In site 5 also a hematite component is present which however, is strongly scattered. In the Jurassic limestones of the sP (sites 2–4,22,113,115,122,127,140,142,144–146,155) remanences are dominated by magnetite and are almost completely removed by AF demagnetisation (after initial heating to 150°C to destroy goethite remances). A one-component behaviour is generally observed. For the Tertiary sediments of the sP mainly TH (sites 11–17,20–21,24,25,27,29–35,107) but also AF (sites 18–19,37) treatment reveals a well grouped magnetite remanence for most sites (Fig. 6a). In site 25, additionally a stable and consistent hematite component occurs (Fig. 6a). Remanence directions of sites 11, 12, 14, 32 and 33 are apparently scattered ($k < 10$). It will be shown later that this scattering is not irregular but represents a small-circle distribution, recording different stages of tectonic displacement. Late Cretaceous red beds of the sP (166,172,174) do not provide significant results.

For the Jurassic limestones of the central Pamirs (cP) (sites 49–55) a nearly complete AF demagnetisation is obtained. Two components are separated, both carried by magnetite (Fig. 6b). The behaviour of the Cretaceous limestones of the cP (sites 42–44) is similar, however only site 43 shows two components; coexisting goethite had to be

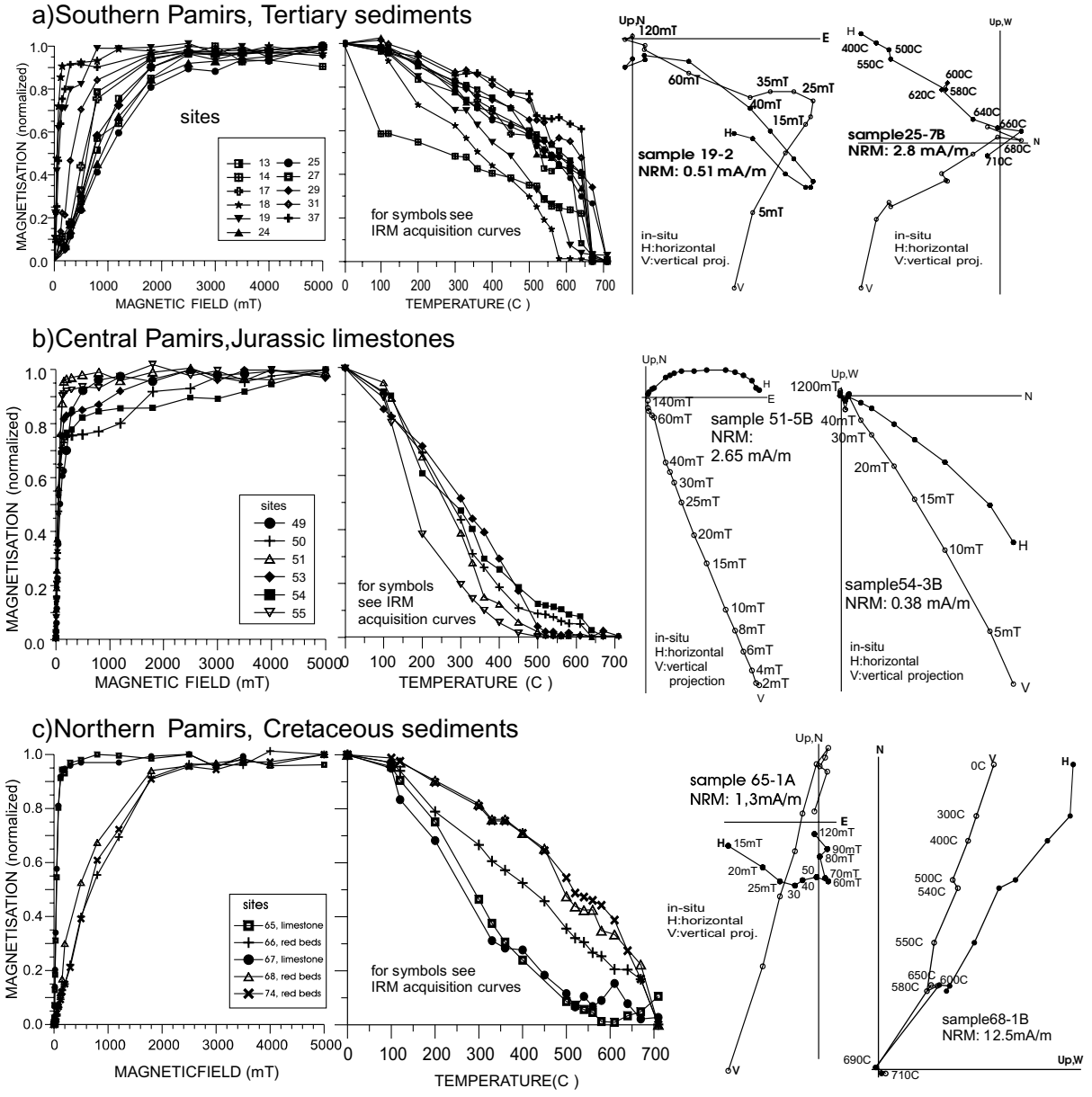

Fig. 6. Examples of rock- and palaeomagnetic measurements. IRM-acquisition, thermal demagnetisation of saturation IRM (SIRM-T) and demagnetisation of NRM. For magnetic mineralogy see Table 2.

destroyed by a first 150°C step. Tertiary red beds of the cP (sites 40–41,45–48) predominantly contain hematite. Thermal demagnetisation identifies also magnetite as a remanence carrier and directions of the magnetite and hematite components cannot be distinguished from each other.

Magnetite is a remanence carrier in the Cretaceous limestones (sites 65,67,74) as well as in the Cretaceous red beds (sites 66,68,79–80) of the northern Pamirs (nP). Hematite dominates in the red beds of the nP but TH treatment shows similar directions of the magnetite and hematite components (Fig. 6c). During AF demagnetisation the Cretaceous limestones of the nP reveal a similar behaviour as the limestones from the central Pamirs, partly with two components (Fig. 6c). Tertiary sediments of the nP (sites 62–64,71,72,78,81–82) behave like Cretaceous red beds during TH cleaning.

In summary, only magnetite components are significant (all results in Table 2 stem from magnetite). Hematite remanences, if identified, either yield the same direction as magnetite or are scattered; they are not further discussed for this reason.

4.3. Fold tests

In most cases, the fold test according to McElhinny (1964) yields a significant result (Table 3). Fold tests according to McFadden (1990) do not provide any additional information. Also, the data have been stepwise

Table 2
Rock- and palaeomagnetic results. All remanences are carried by magnetite. *N*: number of specimens measured, spec. (*p*/*n*): number of specimens used for statistics in geographic coordinates with positive (*p*) and negative (*n*) inclination. Bedding is given as the azimuth and angle of dip. Upright/overturned bedding is identified from cross bedding or other criteria. Ferrimagnetic minerals (as identified from rock magnetic measurements) mt: magnetite, hem: hematite (in brackets if minor amounts). If two remanence components are present, site-no. 1 represents the lower coercive or lower unblocking component, site-no. 2 the higher coercive or higher unblocking component. D_{is}/I_{is} and D_{bc}/I_{bc}: declination/inclination in geographic and bedding corrected coordinates respectively, α_{95}: 95% confidence angle; *k*: precision parameter

Site	Lithology	Geological age	Mean age	Spec.*p*/*n*	Bedding	Upright/Overturned	Ferrimagn.		Demag.	In-situ				Bedding corrected			
							mt	hem		D_{is}	I_{is}	α_{95}	k	D_{bc}	I_{bc}	α_{95}	k
Southern Ppamirs																	
1	Sandstone	Early permian	273	12 11/0	340/67		x		TH	73.1	57.4	10.6	19.7	14.2	23.0	12.3	14.8
2	Limestone	Early to middle Jur.	183	9 8/0	326/26; 162/35		x	(x)	AF	8.6	39.6	9.5	35	13.4	43.7	27.5	5.0
3	Limestone	Early to middle Jur.	183	10 3/5	318/60		x		AF	22.8	36.2	11.0	26.5	5.1	0.1	10.2	30
4	Limestone	Early to middle Jur.	183	8 7/1	334/53		x	(x)	AF	43.6	55.9	17.0	11.6	8.4	19.5	18.4	10.0
5.1	Sandstone	Early permian	273	8 8/0	333/74	Overturned	x		AF	38.8	41.5	10.8	27.4	16.3	−6.3	15.6	13.5
5.2				8 0/4	333/74		x		AF	186.4	−47.5	8.1	130	178.8	25.6	7.8	140
6	Sandstone	Early permian	273	12 11/0	347/78	Overturned	x	x	TH	27.8	35.7	10.0	21.9	24.5	−29.0	10.8	28.7
9	Sandstone	Early permian	273	7 7/0	175/61		x		TH	48.3	39.7	15.9	15.4	115.5	45.8	16.7	14.0
13	Red beds	Tertiary	34	9 7/2	356/18	Upright	x	x	TH	20.4	51.5	12.2	21.5	14.9	35.9	12.1	21.9
15	Red beds	Tertiary	34	11 4/5	043/45		x	(x)	TH	199.2	−15.2	15.5	12.0	197.2	23.0	16.0	11.3
16	Red beds	Tertiary	34	11 0/11	0010/48		x	x	TH	60.8	−9.7	13.7	12.1	79.1	−35.2	13.7	12.1
17	Red beds	Tertiary	34	8 1/6	005/53		x	x	TH	19.6	41.6	8.0	58	16.3	−10.0	8.1	57
18.1	Sandstone	Tertiary	34	9 6/3	334/42	Overturned	x		AF	359.4	45.8	11.6	20.8	351.5	6.4	11.6	20.8
18.2				9 9/0	334/42		x		AF	163.5	−9.3	5.2	100	165.1	32.1	5.2	100
19.1	Sandstone	Tertiary	34	9 7/0	330/36		x		AF	330.6	48.1	14.9	17.3	330.4	12.1	14.9	17.3
19.2				9 9/0	330/36		x		AF	128.2	20.6	10.9	23.5	115.1	52.7	10.9	23.5
22	Limestone	Early to middle Jur.	183	6 6/0	182/43		x	(x)	AF	71.1	55.6	19.9	12.2	130.2	47.8	19.9	12.2
24	Red beds	Tertiary	34	11 11/0	029/41		x	x	TH	239.4	24.4	14.7	12.3	264.1	55.7	14.7	12.3
25	Red beds	Tertiary	34	10 10/0	019/38		x	x	TH	222.0	31.7	9.3	28.0	247.5	63.6	9.3	28.0
27	Red beds	Tertiary	34	8 7/0	183/68		x	x	TH	320.9	38.7	14.3	18.8	238.2	50.5	14.3	18.8
29	Red beds	Tertiary	34	9 6/2	018/43		x	x	TH	213.9	16.4	16.2	12.7	226.6	56.6	16.2	12.7
30	Red beds	Tertiary	34	9 3/6	009/71		x	x	TH	345.8	68.0	12.1	19.2	0.9	−1.2	13.4	15.8
31	Sandstone	Tertiary	34	9 9/0	030/60	Upright	x	x	TH	275.7	65.7	17.5	11.0	2.2	38.0	16.6	12.0
34	Sandstone	Tertiary	34	11 8/0	158/67	Overturned	x	x	TH	275.6	74.3	10.8	27.0	173.8	30.0	12.0	22.4
35	Sandstone	Tertiary	34	11 9/0	343/61	Upright	x	x	TH	226.7	59.6	10.1	17.1	308.0	37.9	17.1	10.1
37	Sandstone	Tertiary	34	12 12/0	205/45		x	(x)	AF	249.3	54.2	9.6	21.3	230.1	16.1	9.6	21.3
107	Red beds	Tertiary	34	9 6/2	004/27		x	x	TH	6.3	43.2	12.0	22.1	5.7	16.2	12.0	22.1
113	Limestone	Middle Jur.	168	9 7/0	342/32		x		AF	48.7	51.4	21.4	10.1	24.2	32.5	21.4	10.1
115	Limestone	Early to middle Jur.	183	10 9/0	328/64		x		AF	45.5	59.6	16.1	11.2	358.9	16.3	16.1	11.2
122	Limestone	Early to middle Jur.	183	11 8/0	179/69		x	(x)	AF	351.7	58.3	18.3	10.1	185.3	52.4	18.3	10.1
127	Limestone	Middle Jur.	168	10 10/0	144/62		x	(x)	AF	293.9	50.7	5.0	93	180.7	57.9	5.0	93
140	Limestone	Early to middle Jur.	183	14 13/0	353/67		x		AF	341.4	36.6	11.5	14.0	342.3	−29.4	11.5	14.0
142	Limestone	Early Jur.	193	9 9/0	055/23		x		AF	61.9	40.1	12.8	17.1	60.5	17.2	12.8	17.1
144	Limestone	Early Jur.	193	10 8/0	162/72		x		AF	343.7	54.0	9.6	34	160.3	53.9	9.6	34
145	Limestone	Early to middle Jur.	183	7 7/0	327/49		x		AF	4.6	42.8	8.2	55	353.6	0.4	8.2	55
146	Limestone	Early to middle Jur.	183	7 6/0	031/42		x		AF	10.2	57.5	8.5	63	19.5	16.9	8.5	63
155.1	Limestone	Early to middle Jur.	183	9 7/0	332/78		x		AF	10.2	54.5	5.4	127	354.0	−16.1	5.4	127
155.2				9 6/0	332/78		x		AF	44.6	33.8	15.7	19.2	25.1	−7.3	15.7	19.2
158	Sandstone	Early permian	273	11 10/0	006/44		x	(x)	AF	335.7	53.3	6.5	57	348.0	12.6	6.5	57
161	Sandstone	Early permian	273	12 12/0	013/59		x	(x)	AF	98.5	67.5	2.8	249	41.8	25.1	4.9	80

Table 2 (*continued*)

Site	Lithology	Geological age	Mean age		Spec.*p*/*n*	Bedding	Upright/Overturned	Ferrimagn.		Demag.	In-situ				Bedding corrected			
								mt	hem		D_{is}	I_{is}	α_{95}	k	D_{bc}	I_{bc}	α_{95}	k
Central Pamirs																		
40	Red beds	Tertiary	34	12	12/0	340/41		x	x	TH	345.3	48.4	7.6	34	347.8	−2.5	7.6	34
41	Red beds	Tertiary	34	10	10/0	340/41		x	x	TH	9.5	36.9	17.8	10.3	2.9	2.7	17.3	9.9
42	Limestone	Late Cretaceous	81	9	3/3	022/27		x		AF	299.9	50.7	12.7	28.7	326.3	40.5	12.8	28.7
43.1	Limestone	Late Cretaceous	81	9	6/0	015/30		x		AF	338.6	45.7	14.5	22.2	348.9	19.8	14.5	22.2
43.2				9	0/6	015/30		x		AF	97.9	−49.3	11.3	36	130.5	−44.2	11.3	36
44	Limestone	Late Cretaceous	81	10	8/1	064/30		x		AF	327.2	67.1	5.4	93	21.4	55.1	5.4	93
45	Red beds	Tertiary	81	9	0/9	011/67		x	x	TH	353.1	−27.6	6.3	68	261.6	−73.2	6.3	68
46	Red beds	Tertiary	81	9	0/9	011/67		x	x	TH	344.0	−14.0	9.9	32	295.6	−63.0	9.9	32
47	Red beds	Tertiary	34	8	0/7	005/34		x	x	TH	299.3	−88.4	13.3	21.5	187.6	−56.6	13.3	21.5
48	Red beds	Tertiary	34	9	0/8	024/40		x	x	TH	65.0	−76.6	10.2	31	186.9	−59.0	10.2	31
49.1	Limestone	Middle to late Jur.	162	8	7/0	032/33		x		AF	32.9	53.3	4.5	185	32.6	20.3	4.5	185
49.2								x		AF	0.3	53.7	3.6	286	12.1	23.7	3.6	286
50.1	Limestone	Middle to late Jur.	162	8	8/0	022/52		x	(x)	AF	50.9	60.1	13.1	18.9	216.2	−10.9	13.1	18.9
50.2					8/0			x		AF	24.7	65.8	2.1	716	23.1	13.9	2.1	716
51.1	Limestone	Middle to late Jur.	162	10	8/0	353/76		x		AF	133.4	55.3	15.8	13.2	20.7	38.6	15.8	13.2
51.2				10	10/0	353/76		x		AF	16.0	68.3	9.8	25.2	1.3	−6.0	9.8	25.2
52.1	Limestone	Middle to late Jur.	162	9	7/0	212/85		x		AF	88.0	54.5	18.2	11.9	180.5	23.2	18.2	11.9
52.2				9	6/1			x		AF	4.6	62.4	9.7	40	226.1	29.2	9.7	40
53.1	Limestone	Middle to late Jur.	162	9	7/0	167/80		x		AF	50.7	69.5	15.9	13.1	146.5	18.1	15.9	13.1
53.2					8/0			x		AF	12.4	38.5	12.5	24.3	130.7	53.0	12.5	24.3
54.1	Limestone	Middle to late Jur.	162	9	7/0	020/54		x	(x)	AF	51.7	58.0	11.4	28.9	36.3	7.7	11.4	28.9
54.2					8/0			x	(x)	AF	23.1	55.6	8.9	40	21.7	1.6	8.9	40
55.1	Limestone	Middle to late Jur.	162	8	6/0	030/61		x		AF	214.1	70.6	18.9	11.2	28.0	48.4	18.9	11.2
55.2					7/0			x		AF	354.7	65.8	9.0	46	16.2	8.6	9.0	46
Northern Pamirs																		
62	Sandstone	Tertiary	34	12	11/0	040/40	Upright	x	x	TH	51.6	74.3	11.3	17.2	43.8	34.6	11.3	17.2
63	Red beds	Tertiary	34	15		220/80	Upright				245.8	27.2			254.4	−45.9	10.9	31.6
64	Red beds	Tertiary	34	10	7/0	050/54	Upright	(x)	x	TH	219.1	78.6	17.8	12.5	54.3	45.5	17.1	13.4
65.1	Limestone	Early Cretaceous	122	10	9/0	212/53	Overturned	x		AF	124.9	−70.4	10.3	25.9	56.3	−35.3	10.3	25.9
65.2				10	0/9			x		AF	354.9	47.4	7.8	44	269.2	61.0	7.8	44
66	Red beds	Late Cretaceous	81	12	12/0	203/19		(x)	x	TH	21.9	63.9	13.1	11.9	19.0	82.9	13.1	11.9
67	Limestone	Early Cretaceous	81	18	17/0	279/25		x		AF	349.3	55.3	8.0	30	329.0	45.7	7.8	32
68	Red beds	Late Cretaceous	81	12	12/0	193/75	Upright	x	x	TH	44.6	27.2	9.8	22.9	121.1	57.8	9.9	22.4
71	Red beds	Tertiary	34	10	1/8	022/85	Overturned	x	x	TH	318.9	−32.8	17.1	10.0	257.9	−25.2	17.1	10.0
74	Limestone	Early Cretaceous	122	9	7/0	032/85	Overturned	x	x	TH	207.9	−27.8	17.1	13.5	205.4	57.0	17.1	13.5
78	Red beds	Tertiary	34	12	7/0	122/68		x	x	TH	323.7	40.4	18.0	12.2	82.7	64.3	18.0	12.2
79	Red beds	Late Cretaceous	81	13	10/1	150/34		x	x	TH	317.0	38.2	14.4	11.0	298.7	70.2	14.4	11.0
82	Sandstone	Tertiary	34	11	10/0	140/27		x	(x)	TH	329.5	61.7	10.5	22.1	38.2	85.4	10.5	22.1

Table 3
Summary of fold tests (according to McElhinny, 1964), and stepwise unfolding. Results for site means (*N*, number of site means) are presented if the level of 95% significance is exceeded. Otherwise, the fold test with individual specimen directions (*n*, number of specimens) is shown. Dec., declination; Inc., inclination; α_{95}, 95% confidence angle; *k*, precision parameter; k_{max} at % unfolding: maximum of the *k*-value over the range of unfolding from −50 to 150%

Group	Sites	*N*	*n*	In-situ				Bedding corrected				Fold test	k_{max} at % of unfolding
				Dec.	Inc.	α_{95}	*k*	Dec.	Inc.	α_{95}	*k*		
Southern Pamirs													
Permian sandstones	1,5.1,6,9	4		44.5	44.6	18.5	25.6	3.8	−15.8	59.9	3.3	Neg. 99%	0
Jurassic limestones	2a,2b,3,4,113,115,122, 140,142,144,145,146,155	9		16.4	50.9	10.0	18.1	7.6	3.0	22.4	4.4	Neg. 99%	0
Tertiary sediments western group	13,14,24,25,27,29,30, 31,34,35,37,107		107	264.6	62.8	7.7	4.2	219.7	37.3	10.0	2.9	Neg. 95%	18
Tertiary sediments eastern group	15,16,17,18.2,19.2	5		186.5	−8.8	52.9	3.1	190.7	39.2	44.3	3.9	Indiff.	Not reached within range of unfolding
Central Pamirs													
Jurassic limestones	49–55												
Low coercive components			52	71.6	68.7	7.5	8.0	20.4	14.1	10.3	4.6	Neg. 95%	12
High coercive components		7		10.8	59.8	8.9	47.3	14.2	−5.6	28.8	5.3	Neg. 99%	9
Cretaceous limestones	42,43,44		21	120.8	−59.0	7.2	20.5	161.2	−52.2	9.9	11.2	Neg. 95%	Not reached within range of unfolding
Tertiary red beds western group	45,46,47,48		32	354.4	−51.7	12.6	5.0	225.9	−71.4	7.9	11.2	Pos. 99%	Not reached within range of unfolding
Northern Pamirs													
Cretaceous limestones & red beds, eastern group	65,66,67,68,74		56	13.7	48.2	6.9	8.6	307.2	78.2	9.6	4.9	Neg. 99%	−9
Tertiary sediments	62,64,71		27	127.0	70.5	13.3	5.3	58.3	35.3	9.3	9.8	Pos. 95%	129

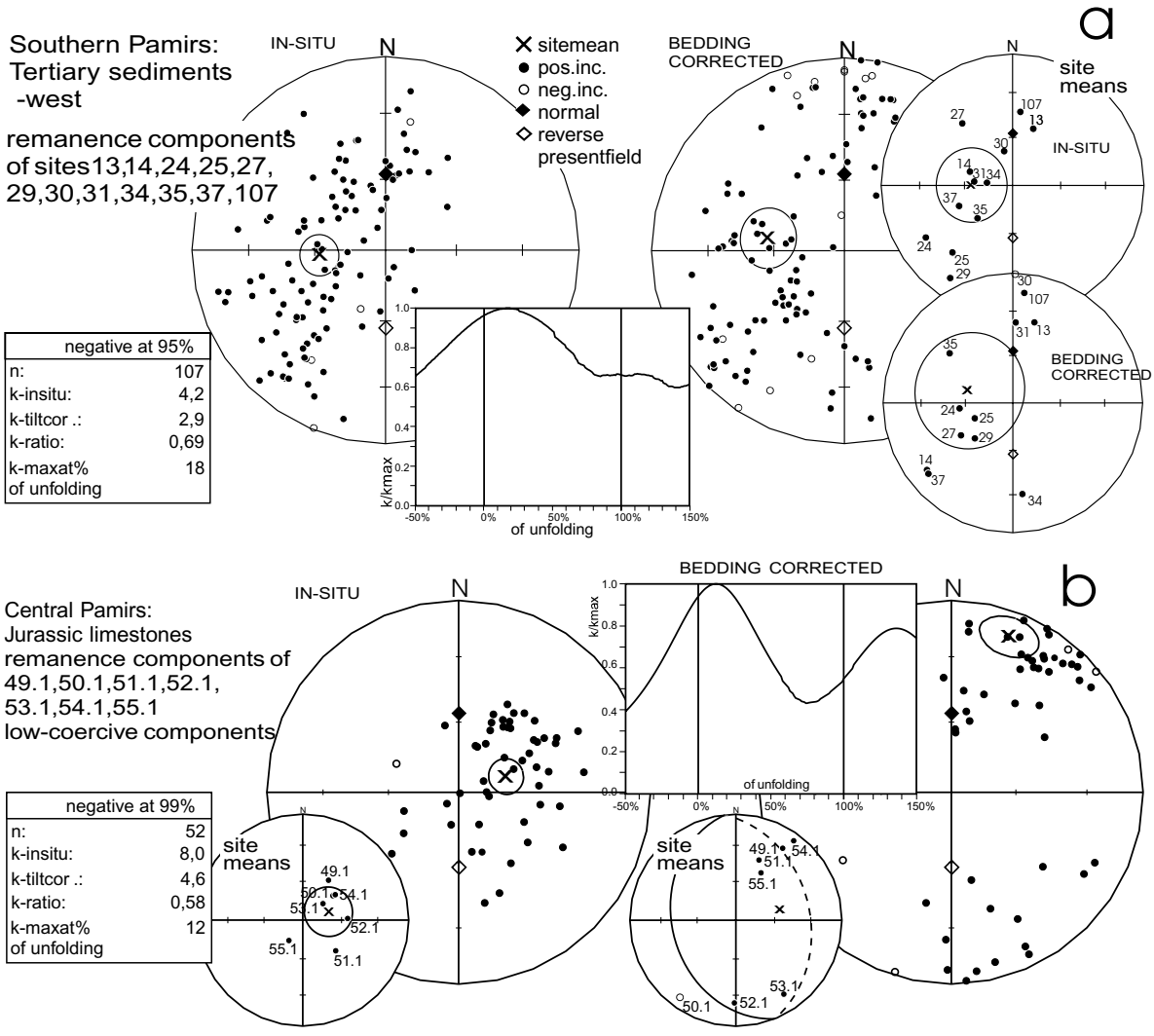

Fig. 7. Remanence directions and fold tests for (a) Tertiary sediments in the southern Pamirs and (b) Jurassic limestones in the central Pamirs. In-situ and bedding corrected remanence directions are shown (large equal area plots: single specimen directions; small equal area plots: site mean directions). Results of fold tests (according to McElhinny, 1964) are listed in the small tables (*n*, number of specimens; *k*, precision parameter). the *k*-ratio for stepwise unfolding is also shown. Stereographic projection is chosen in this figure.

unfolded (from −50 to +150% unfolding). Although most of the rocks do not exhibit macroscopic signs of metamorphism, their remanences clearly indicate a secondary, synfolding character. Two examples of the fold tests are shown in Fig. 7, and relevant results are listed in Table 3. For the Jurassic limestones of the central Pamirs, a series of fold tests have been applied on both, high and low coercive components. Six of them are clearly secondary, one is indifferent, and two indicate a pre-folding remanence character. However, the statistically positive fold tests are considered to be misleading, as maximum k values are reached far from 100% of unfolding. It is shown later by small circle analysis, i.e. by backtilting angles bt, that the apparently pre-folding remanences are at least in part secondary. However, a few are likely to be pre-folding, maybe even primary, which is indicated by bt angles equal to tectonic tilt angles (sites 42, 43.2 and 47, 48 and 51.1, 55.1).

4.4. Small circle distributions

Remanences from 12 Tertiary sites of the southern Pamirs (Fig. 7a) show the tendency of a small circle distribution. Examining single sites, we can find a clear small-circle distribution of specimen directions (Fig. 8); three of these sites have a *k*-value below 10. Their remanence components have been obviously acquired at different stages of folding, thus recording a continuous path of displacement. For the tectonic reconstruction, a mean small circle has been calculated using a parametric model of a 1D Gaussian distribution of the angular distances *d* parallel to the tilt axis (see Table 4). This has been done by averaging the *d*-angles (arccos *d*) of each remanence direction arithmetically and calculating a 95%-confidence interval as usual. The symmetric confidence interval of the *d*-angle results in an asymmetric interval for the block rotation.

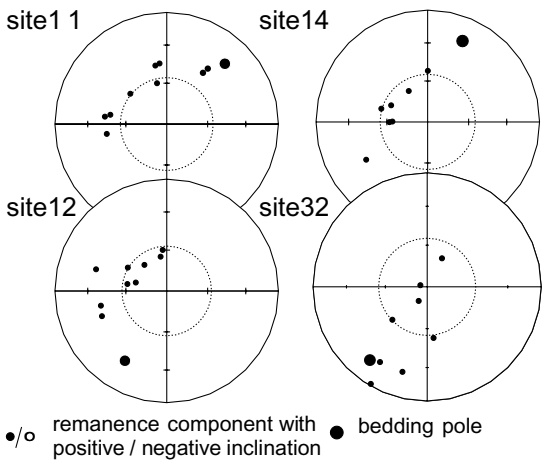

Fig. 8. Small-circle distribution of single specimen directions parallel to the tilting direction in four sites (having uniform bedding). Remanence components have different ages, thus recording a displacement path. Note that upright (sites 12,32) and overturned bedding (sites 11,14) can be inferred by comparing the present bedding with the tilt of the remanences. Stereographic projection is chosen in this figure.

5. Tectonic interpretation

5.1. Remanence age

Secondary overprinting seems to prevail in nearly all sampled rocks throughout the Pamirs. Geochronological cooling ages (Schwab et al., 1999) indicate a metamorphic event around 20 Ma in the central and southern Pamirs.

However, temperatures were probably to low in most samples to explain remagnetisations by thermal overprint. An alternative explanation would be a hydrothermal influence, i.e. a chemical remanence produced by newly formed ferrimagnetic phases associated with fluid migration through the rock. Progressive growth of new magnetite may explain the record of a displacement path as shown above (Fig. 8) as different particles exceed the superparamagnetic to single domain grain size transition at different geological times during folding. Nevertheless, the exact age of remanence acquisition is not very critical for further interpretations. The expected palaeofield direction did not change much between 10 and 40 Ma (Fig. 2) and thus deviations from the assumed age of 20 Ma would have to be large to affect the results for bt and br significantly.

5.2. Palaeoinclination and crustal shortening

Using the APWP of stable Eurasia from Besse and Courtillot (1991; pole at 20 Ma: 147.6°E/82.3°N, $A95 = 3.3°$), the corresponding palaeofield direction for the target area is expected to be $D/I = 10 \pm 6°/59 \pm 3°$. The minimum amount of Cenozoic northward displacement of the Pamirs due to crustal shortening is estimated to be 300 km (Burtman and Molnar, 1993). Hence, the inclination at 20 Ma ago should be ~56°.

The inclination at the time of remanence acquisition can be assessed from the angular distances d of the in situ site mean directions. Values of d define the upper limit for the inclination of the acquisition field I_{acq}, according to Eq. (2). Fig. 9 depicts the distribution and cumulative distribution of the maximum I_{acq} ($I_{acq\ max}$) of the site means for all investigated sites of the whole Pamirs as well as the southern Pamirs alone. The cumulative number of sites increases significantly above an $I_{acq\ max}$ of around 55–58° (whole Pamirs) or 55° (southern Pamirs). Comparison of $I_{acq\ max} = 55°$ with the expected palaeofield inclination of (~59 ± 3°) indicate a difference of 4°, implying that ~450 km of northward displacement has taken place since the time of remanence acquisition. This amount is well within the range of 300–700 km northward displacement of the Pamirs during Cenozoic as reported by Burtman and Molnar (1993).

Six sites in Fig. 9 give an $I_{acq\ max}$ lower than 55° (sites 16,71,3,5.1,43.2,42). This indicates that remanence acquisition has occurred at lower latitudes. For sites 16, 71, and 5.1 (Tertiary), a primary origin is uncertain because the inclination in stratigraphic coordinates is much shallower than expected for the Tertiary (see Table 2 and Fig. 2). Rotation around an inclined axis, inclination shallowing, or other rockmagnetic effects may account for it. A primary origin seems to be possible for sites 43.2 and 42 (Cretaceous) because their bedding corrected inclinations are well within the range expected for the area (see Table 2 and Fig. 2). However, a negative fold test for sites 42, 43.2 and 44 (95% significant) suggests a secondary origin.

5.3. Small-circle reconstruction of the block rotation

Small circle reconstruction has been applied as described in the sections '*The small circle reconstruction*' and '*Example for small circle reconstruction*'. A reference field of was selected for the southern and central Pamirs, $D/I = 10°/57°$ for the northern Pamirs, and $D/I = 10°/60°$ in the Alai (based on expected values from the APWP and taken into account shortening within Eurasia). All sites with an $I_{acq\ max}$ below 55° were excluded from further processing. From the four alternative reconstructions the one with the shortest total rotation was selected as the most probable solution. Results are listed in Table 4. Most site means do not seem to have undergone large tilting. In most sites, the selected reconstruction is by far the most probable solution with respect to angles of backtilting and block rotation. Only for site 78, two solutions have a similar probability.

Pre-folding (primary?) remanences may exist in sites 44, 47 and 48 where untilting is near to 100% of the present dip of bedding. In contrast, the apparently primary sites 62, 64 and 71 (see fold tests in Table 3) are far from 100% untilting.

6. The tectonic setting: block rotations vs. tilting directions

For each site, a reconstructed tilt axis and a block rotation

Table 4
Results from small-circle reconstruction (backtilting and block rotation). Only the most probable solution is listed. az./dip, azimuth/angle of dip; bedding, upright or overturned (overt.) bedding derived from field evidence; *d*, angular distance (see Fig. 3), $I_{acq\ max.}$: maximum palaeoinclination; % of untilting, percent of untilting related to the present dip (assumed to be upright); remark, bedding determined by comparison of the present bedding with the sense of untilting assuming that tilting did not reverse direction (upright or overturned, indiff. when angle of untilting is below ±10°, >dip when angle of untilting exceeds dip for either upright or overturned position by more than 10°). $\alpha_{95}/\cos(I_{acq})$: confidence interval of the declination for sites with a Fisher mean (for the small-circle distributions α_{95} of the *d* angle distribution is given)

Site	Dip az (°)	Dip (°)	Bedding (field)	*d*	*d*-angle	I_{acq} max. (°)	Back-tilting (°)	Block-rotation (°)	Reconstruction point		% of untilting	Remark	$\alpha_{95}/\cos I_{acq}$ (°)
									D(°)	*I*(°)			
Southern Pamirs													
1	340	67	–	0.54	122.5	57.5	−16	−40	50	55	23	Upright	18.5
2a	162	35	–	0.38	112.4	67.6	14	−14	24	55	41	Upright	20.6
2b	326	26	–	0.50	120.2	59.8	29	−17	27	55	−112	Overt.	16.6
3	318	60	–	0.73	136.9	43.1							
4	334	53	–	0.53	121.7	58.3	−2	−30	40	55	5	In diff.	29.6
5.2	333	74	–	0.37	111.8	68.2	9	−3	193	−55	−13	In diff.	14.1
6	347	78	–	0.53	122.0	58.0	32	−45	55	55	−41	Overt.	17.4
9	181	61	–	0.57	124.4	55.6	33	−71	81	55	53	Upright	32.5
13	356	18	upright	0.26	104.9	75.1	4	−13	23	55	−22	Indiff.	21.3
15	43	45	–	−0.39	67.1	67.1	46	10	0	55	−103	Overt.	27.0
16	10	48	–	0.76	139.8	40.2							
17	5	53	–	0.19	100.9	79.1	14	−14	24	55	−26	Overt.	13.9
18.1	334	42	–	0.30	107.4	72.6	10	5	5	55	−25	Overt.	20.2
18.2	334	42	–	0.16	99.4	80.6	47	20	170	−55	−111	Overt.	9.1
19.1	330	36	–	0.01	90.4	89.6	7	39	331	55	−19	Indiff.	26.0
19.2	330	36	–	0.35	110.3	69.7	83	77	113	−55	−230	Overt.	19.0
22	182	43	–	0.53	121.9	58.1	−2	−59	69	55	−4	Indiff.	34.7
24	29	41	–	−0.46	62.6	62.6	−85	34	336	55	207	> Dip	25.6
25	19	38	–	−0.33	70.6	70.6	−86	26	344	55	226	> Dip	16.2
27	183	68	–	−0.52	58.5	58.5	27	73	297	55	39	Upright	24.9
29	18	43	–	−0.26	74.8	74.8	−105	19	351	55	244	> Dip	28.2
30	9	71	–	−0.15	81.5	81.5	−14	16	354	55	19	Upright	21.1
31	30	60	–	−0.38	68.0	68.0	−39	21	349	55	64	Upright	30.5
34	158	67	Overt.	−0.24	76.1	76.1	−25	57	313	55	−37	Overt.	18.8
35	343	61	Upright	−0.45	63.0	63.0	−38	79	291	55	62	Upright	17.6
37	205	45	–	−0.41	65.9	65.9	−54	30	340	55	−119	Overt.	16.7
107	4	27	–	0.03	91.7	88.3	12	3	7	55	−44	Overt.	20.9
113	342	32	–	0.57	125.0	55.0	16	−59	69	55	−49	Overt.	37.3
115	328	64	–	0.49	119.6	60.4	−12	−17	27	55	19	Upright	28.1
122	179	69	–	−0.07	86.2	86.2	−3	18	352	55	−5	Indiff.	31.9
127	144	62	–	−0.32	71.5	71.5	5	80	290	55	8	Indiff.	8.7
140	353	67	–	−0.16	80.7	80.7	19	33	337	55	−28	Overt.	20.0
142	55	23	–	0.09	95.3	84.7	15	−54	64	55	−65	Overt.	22.3
144	162	72	–	0.02	91.0	89.0	1	26	344	55	1	Indiff.	16.7
145	327	49	–	0.45	116.6	63.4	17	−8	18	55	−34	Overt.	14.3
146	31	42	–	−0.19	79.0	79.0	−3	−2	12	55	6	Indiff.	14.8
155	332	78	–	0.36	111.0	69.0	1	−1	11	55	−1	Indiff.	9.4
158	6	44	–	−0.30	72.5	72.5	2	36	334	55	−5	Indiff.	11.3
161	13	59	–	0.38	112.4	67.6	−26	−45	55	55	44	Upright	4.9

Table 4 (*continued*)

Site	Dip az (°)	Dip (°)	Bedding (field)	*d*	*d*-angle	I_{acq} max. (°)	Back-tilting (°)	Block-rotation (°)	Reconstruction point		% of untilting	Remark	$\alpha_{95}/\cos I_{acq}$ (°)
									D(°)	*I*(°)			
Sites with small-circle distribution													α_{95}
11	223	64	–	−0.50	60.2	60.2		27				Overt.	4.4
12	21	62	Upright	−0.49	60.7	60.7		48				Upright	10.5
14	203	68	Overt.	−0.43	64.5	64.5		36				Overt.	6.2
32	39	70	Upright	0.03	92.0	88.0		−32				Upright	14.3
Central Pamirs													$\alpha_{95}/\cos l_{seq}$
40	353	51	–	−0.09	84.9	84.9	7	26	344	55	−13	Indiff.	13.3
41	340	41	–	0.39	113.2	66.8	22	−13	23	55	−54	Overt.	31.0
42	22	27	–	−0.63	51.1	51.1							
43.1	15	30	–	−0.41	65.5	65.5	12	41	329	55	−41	Overt.	25.3
43.2	15	30	–	0.65	49.7	49.7							
44	64	30	–	−0.39	67.3	67.3	−30	−12	22	55	101	Upright	9.4
45	11	67	–	0.27	105.8	74.2	−93	−29	219	−55	139	> Dip	11.0
46	11	67	–	0.44	116.1	63.9	−99	−51	241	−55	147	> Dip	17.3
47	5	34	–	0.03	91.5	88.5	−36	2	188	−55	105	Upright	23.2
48	24	40	–	−0.15	81.3	81.3	−44	1	189	−55	111	Upright	17.8
49.1	32	33	–	−0.01	90.5	89.5	−2	−23	33	55	5	Indiff.	7.8
49.2	32	33	–	−0.31	71.9	71.9	2	11	359	55	5	Indiff.	6.3
50.1	22	52	–	0.24	103.9	76.1	−6	−37	47	55	11	Indiff.	22.8
50.2	22	52	–	0.02	91.1	88.9	−11	−14	24	55	21	Upright	3.7
51.1	353	76	–	0.36	111.3	68.7	−57	−22	32	55	74	Upright	27.5
51.2	353	76	–	0.14	98.3	81.7	−14	2	8	55	18	Upright	17.1
52.1	212	85	–	0.48	118.8	61.2	1	−79	89	55	1	Upright	31.7
52.2	212	85	–	−0.21	77.7	77.7	−8	0	10	55	−10	Indiff.	16.9
53.1	167	80	–	0.31	108.3	71.7	−21	−10	20	55	−26	Overt.	27.7
53.2	167	80	–	0.34	109.6	70.4	19	−13	23	55	24	Upright	21.8
54.1	20	54	–	0.28	106.2	73.8	−4	−39	49	55	6	Indiff.	19.9
54.2	20	54	–	0.03	91.8	88.2	−1	−13	23	55	1	Indiff.	15.5
55.1	30	61	–	−0.02	88.6	88.6	−54	−18	28	55	89	Upright	33.0
55.2	30	61	–	−0.24	76.3	76.3	−12	4	6	55	20	Upright	15.7
Northern Pamirs and Alai													
62	40	40	Upright	0.05	93.1	86.9	−18	−36	46	57	44	Upright	20.7
64	50	54	Upright	0.04	92.1	87.9	−44	−44	54	57	82	Upright	32.7
65.1	212	53		−0.34	70.4	70.4	−26	16	174	57	−49	Overt.	18.9
65.2	212	53		−0.41	65.9	65.9	13	27	343	57	25	Upright	14.3
66	203	19	–	−0.01	89.5	89.5	−7	−12	22	57	−36	Indiff.	24.1
67	279	25	–	0.54	122.4	57.6	7	11	359	57	12	Indiff.	14.7
68	193	75	Upright	0.47	117.8	62.2	40	−62	72	57	54	Upright	18.0
71	22	85		0.75	138.6	41.4							
74	32	85	Overt.	−0.06	86.4	86.4	29	−29	205	−57	−34	Overt.	31.4
78	122	68		0.28	106.4	73.6	21	34	336	60	which?		36.0
79	150	34	–	−0.18	79.8	79.8	20	59	311	57	57	Upright	26.4

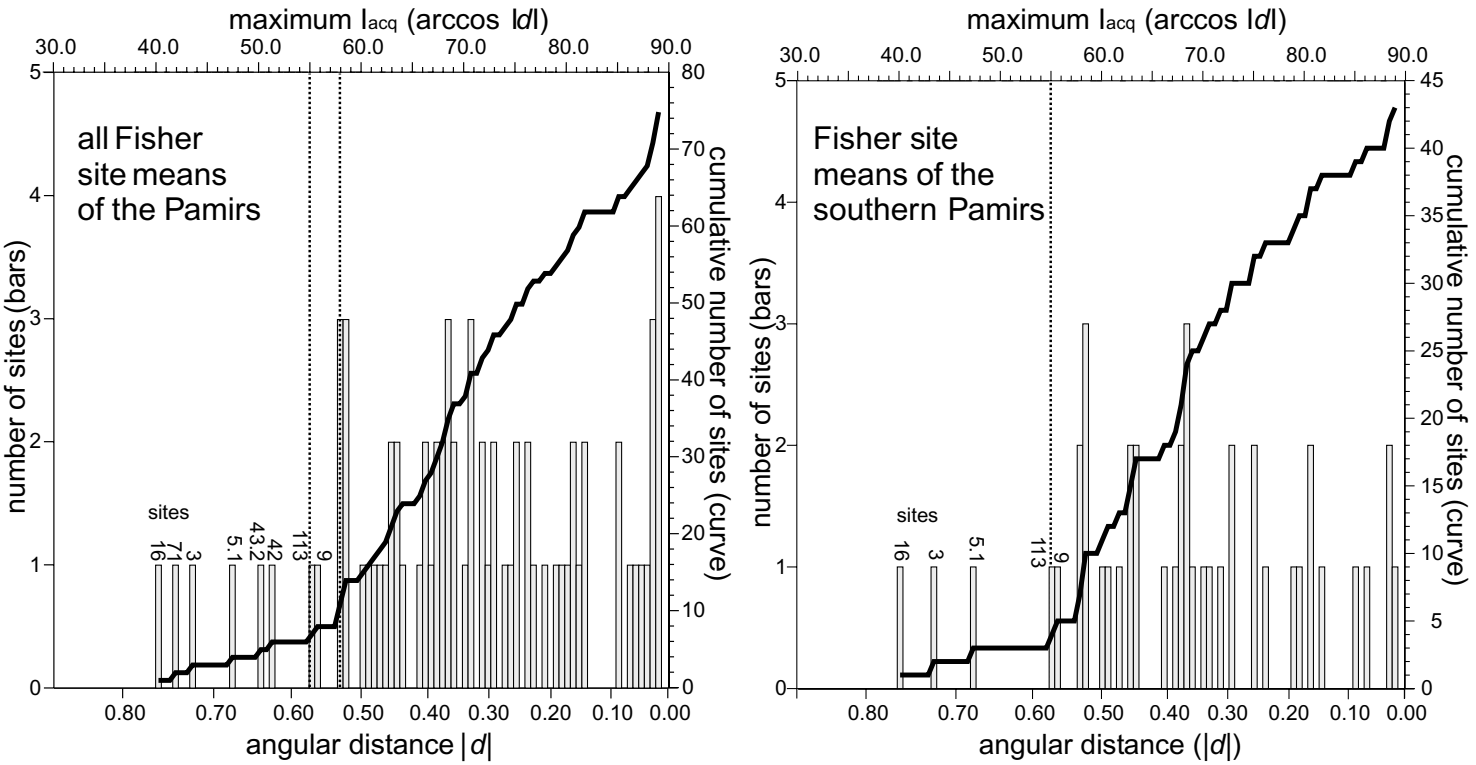

Fig. 9. Histogram and cumulative curve for the distribution of the maximum I_{acq} ($I_{acq\ max}$) (inclination of remanence acquisition field) for all sites from the Pamirs (left) and from the southern Pamirs (right). Details are listed in Table 4. Scale of $I_{acq\ max}$ is linear. Bars refer to the number of sites having an $I_{acq\ max}$ within a range of 0.5°. See text for further explanations.

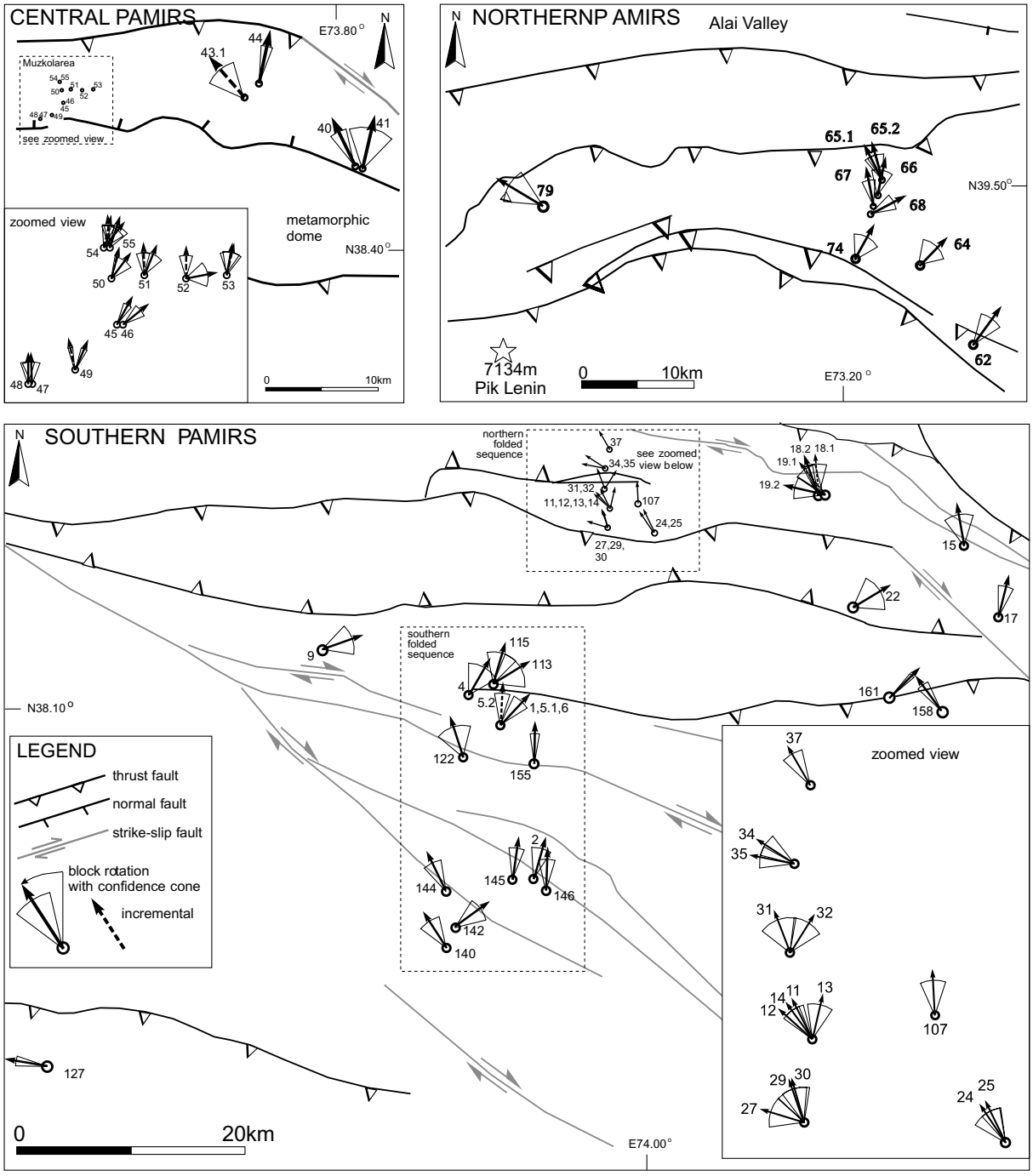

Fig. 10. Palaeomagnetic rotations vs. north for the investigated areas in the southern, central and northern Pamirs. See Fig. 5 for overview. Dashed arrows indicate increments of rotation. For confidence intervals see Table 4.

have been obtained using the corresponding reference field. In the following the tilting directions rather than the tilt axes will be considered (see Fig. 3).

In the S-part of the southern Pamirs (the southern folded sequence in Fig. 10), palaeomagnetic rotations vary and do not show a systematic trend. In the northern folded sequence (i.e. closer to the metamorphic dome) a counterclockwise trend can be seen. In the central Pamirs, palaeomagnetic rotations of sites 40–44 are scattered, while in the Muzkol area they reveal a clockwise rotation. In the northern Pamirs, declination arrows predominantly follow the trend of the thrusts, typical for oroclinal bending.

No clear tectonic setting (oroclinal bending or dextral shear) can be recognised from palaeomagnetic rotations in the southern and central Pamirs. The tilting directions, however, reflect a consistent behaviour of the southern

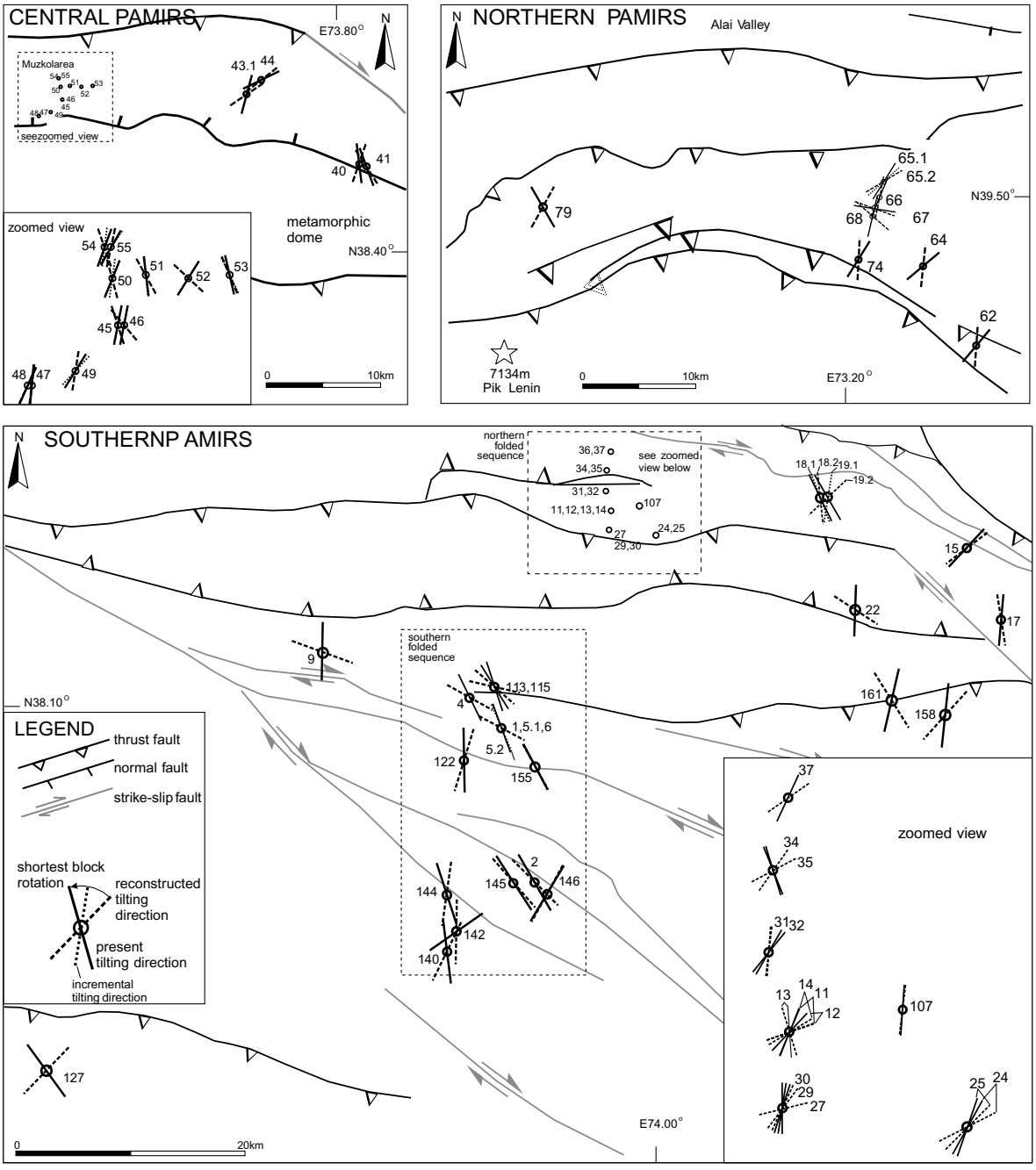

Fig. 11. Present and reconstructed tilting directions for the investigated areas in the southern, central and northern Pamirs.

and the central Pamirs:

- The present tilting directions are oriented closer towards north than the reconstructed ones (Fig. 11).
- The scatter of the reconstructed tilting directions is higher than that of the present tilting directions (Fig. 12).

This is true for larger units (e.g. southern Pamirs) as well as for single folded sequences (e.g. Muzkol area). In contrast to oroclinal bending, which rotates the tilting directions away from the overall convergence direction (by this increasing the scatter; possibly true in the northern Pamirs), they have been rotated towards it (by this decreasing the scatter) (Fig. 13). Probably, N–S shortening has caused the block rotations in the southern and central Pamirs. This observation may reflect a general mechanism in the process of folding: with increasing amount of shortening, the layers in a folded sequence must line up perpendicular to the shortening direction. In the Pamirs, this observation is further supported by evidences reported in the geological map, i.e. that the

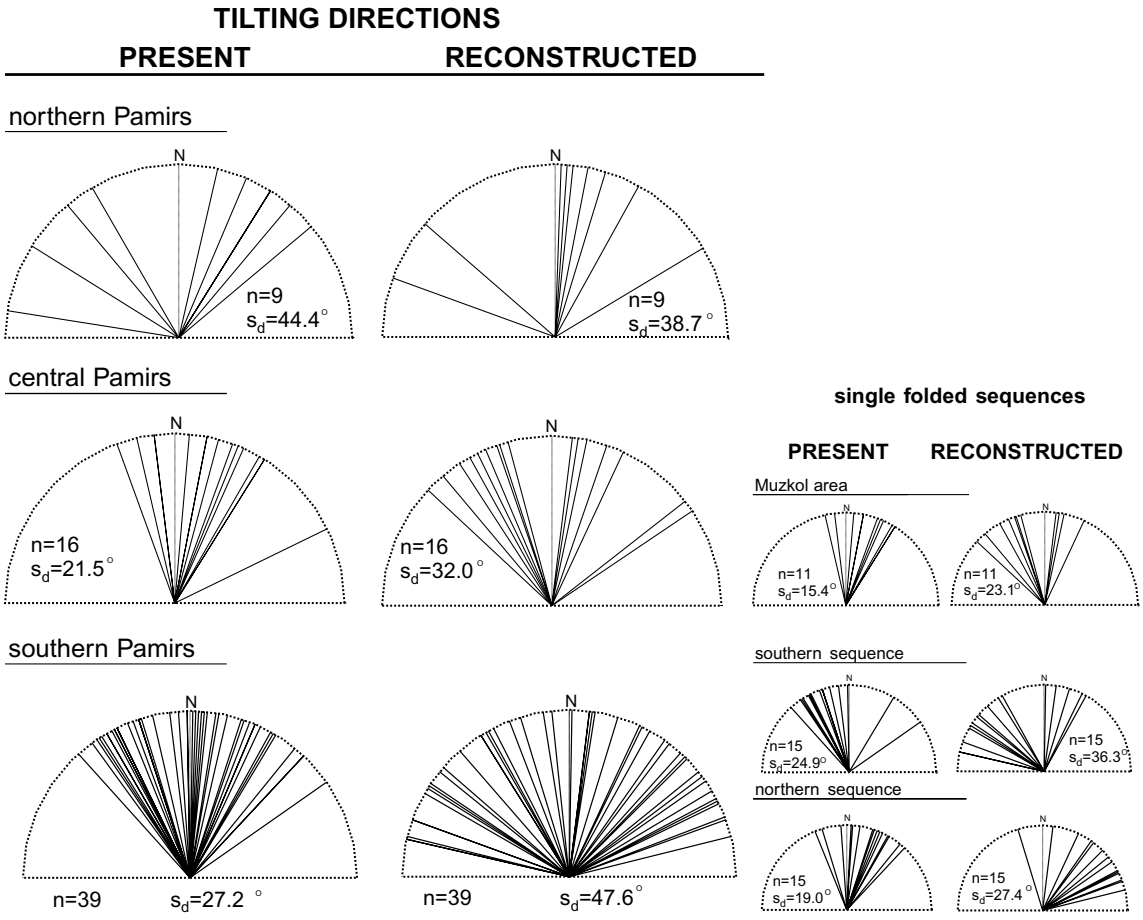

Fig. 12. Tilting directions in equal-area plots with number of sites ($_n$) and standard deviation of the azimuth (s_d). In the southern and central Pamirs, tilting directions show a higher variation at the time of remanence acquisition. In the northern Pamirs, the scatter of the reconstructed tilting directions is relatively lower, indicating an oroclinal bending. For site locations see Figs. 5, 10 and 11.

structures in the southern Pamirs as well as the metamorphic dome are trending rather straight in E–W direction until they are cut by the Pamir–Karakorum fault. If oroclinal bending had occurred in this area, they should be bent.

7. Quantification of N–S shortening

As the block rotations depend on the initial tilting directions as well as the direction and amount of convergence,

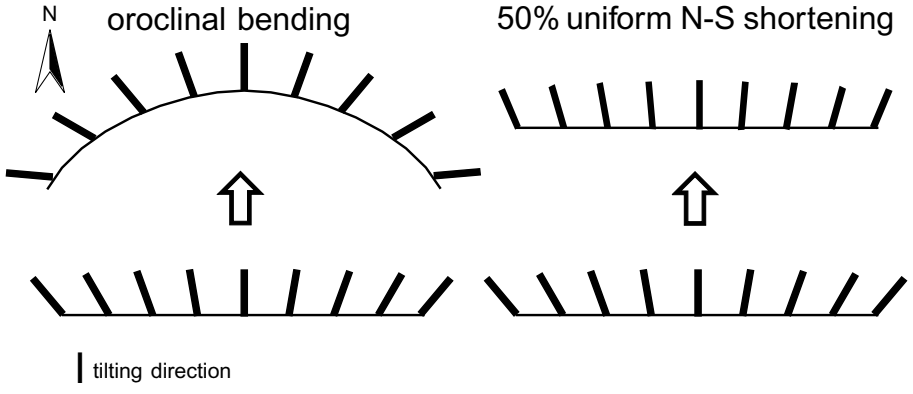

Fig. 13. Oroclinal bending in a N–S convergence regime rotates the tilting directions away from north, thus increasing the scatter. Uniform N–S shortening rotates them towards north reducing the scatter.

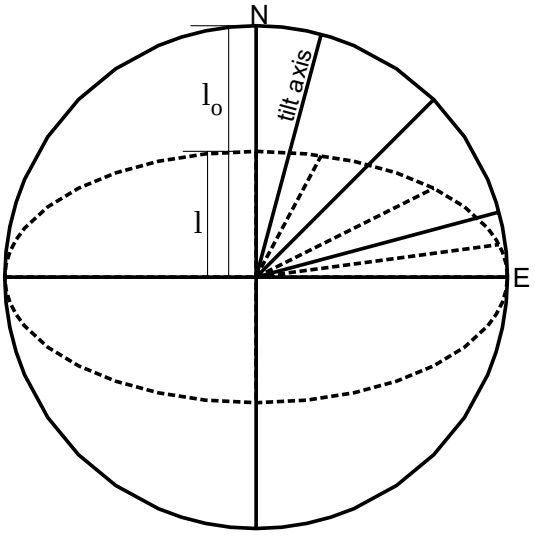

Fig. 14. Rotation of the tilt axes, where N–S shortening is completely taken up by folding (vertical extension). Solid lines show the initial geometry (circle); dashed lines (ellipsoid) result after 50% N–S shortening. For explanation of l/l_0 see Eq. (5).

shortening can be quantified if its direction is known. The estimation of a N–S shortening is acceptable in the overall tectonic setting of this part of the India–Asia collision zone. For the quantification of N–S shortening the following simple approach can be applied:

The reconstructed tilt axes are subjected to uniaxial N–S shortening until their standard deviation around a mean direction reaches the present value. N–S shortening is assumed to be taken up completely by folding, leading to vertical extension (Fig. 14).

The azimuth t'' of a tilt axis after N–S shortening is:

$$t'' = \arctan(\tan t'/(l/l_0)) \quad (5)$$

Here t' is the azimuth of reconstructed tilt axis, l_o is the original length, and l is the length after shortening.

This procedure is applied to the data set of reconstructed tilt axes by iteration until the value of the standard deviation of the azimuths of the tilt axes reaches the present value. Table 5 lists the results for four groups of sites shown in Figs. 11 and 12.

The resulting amount of 63% shortening for the southern Pamirs can be compared to data for Cenozoic shortening reported in the literature. At present, the whole southern Pamirs have a N–S extent of ~100 km. From fault displacements and balanced cross sections, at least 240 km of shortening have been calculated by Burtman and Molnar (1993; and references therein), resulting in an original N–S extent of 340 km. If 100 km are the result of shortening by ~63%, the original length was ~260 km, somewhat below the estimate of 340 km. The shortening reported by Burtman and Molnar (1993) accounts for the total effect of folding and fault displacements in Cenozoic times, while the palaeomagnetic record started at a time when a significant amount of folding was already achieved. Therefore, ~4° (450 km) northward displacement of the southern Pamirs since 20 Ma seems to be an acceptable estimate.

8. Synthesis

Fig. 15 sketches a restoration of the original N–S extent of the southern and central Pamirs, and the amounts of shortening. Since 20 Ma, ~450 km of N–S convergence have been estimated between the southern Pamirs and stable Eurasia using the maximum angular distances of the site mean directions. From this total amount, ~170 km have been consumed by internal shortening in the southern (~160 km) and central Pamirs (~10 km). If shortening within the metamorphic dome and the northern Pamirs is neglected, the remaining 280 km provide a maximum estimate for overthrusting of the Pamirs on Eurasia.

Most of the northern Pamirs consist of granitic and metamorphic rocks consolidated in the Palaeozoic, so it seems unlikely, that this part experienced much internal shortening. It appears plausible that the northern Pamirs acted as a rigid block, against which the central and southern Pamirs have been pushed in the course of progressive indentation. This could be explained by the high amounts of N–S shortening and the absence of oroclinal bending in the southern Pamirs. The amounts of shortening as mentioned above must be treated as rough estimates. However, the following sequence of events seems to be plausible (Fig. 15):

- Northward convergence first affected the southern and central Pamirs and pushed them against the rigid block of the northern Pamirs. This resulted in strong internal

Table 5
Finite N–S oriented uniaxial shortening in the Pamirs ($1 - l/l_0$; l_0 original length, l length after shortening)

Tilt axes from	Standard at present	Deviation (°) reconstructed	Finite shortening by ($1 - l/l_0$)
All sites of the southern Pamirs (39 sites)	27.2	47.6	0.63
Southern folded sequence (15 sites)	24.9	36.3	0.50
Northern folded sequence (15 sites)	19.0	27.4	0.59
Muzkol zone (11 sites)	15.4	23.1	0.39

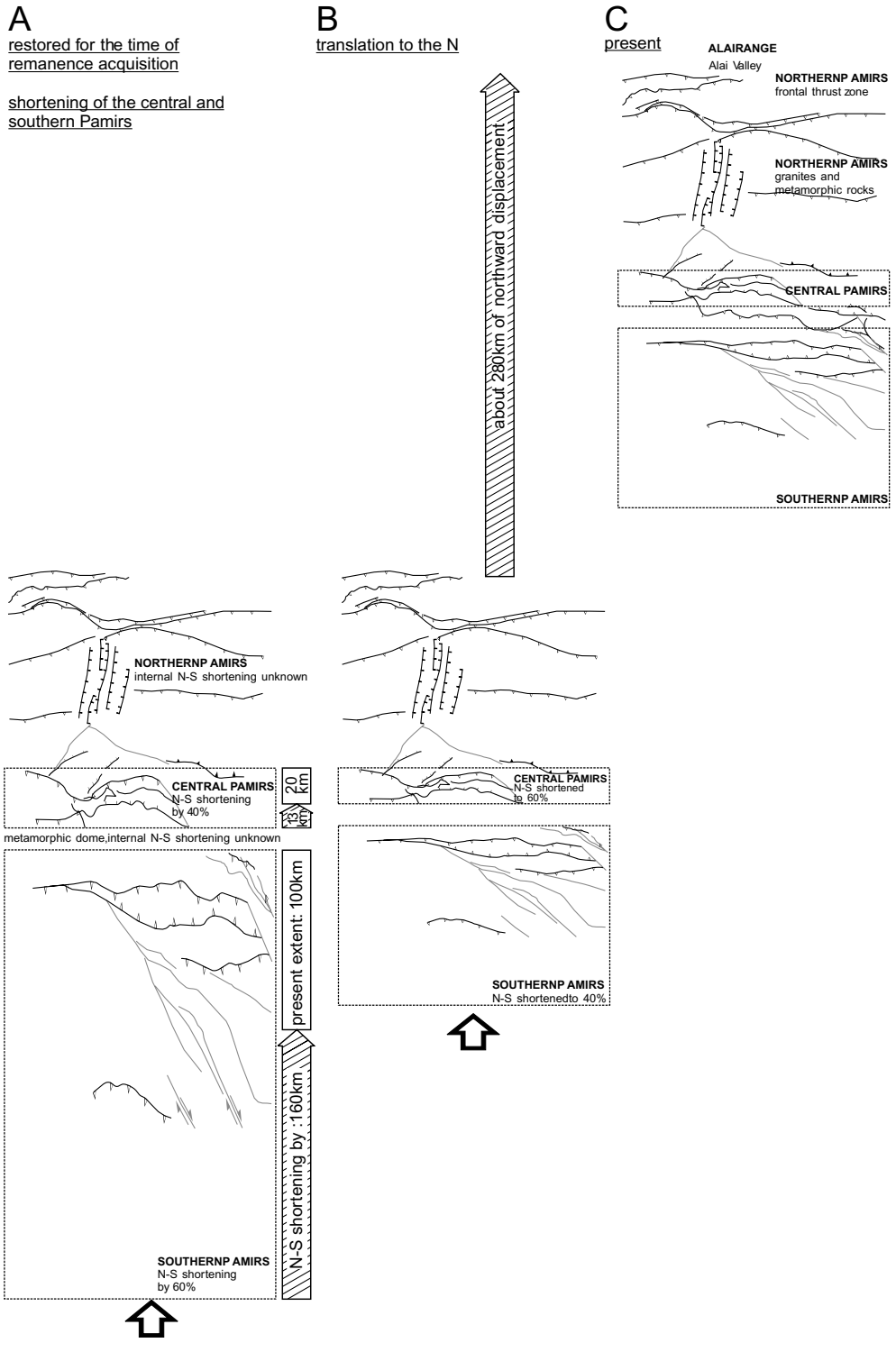

Fig. 15. Schematic sequence of tectonic events. Total shortening between the southern Pamirs and stable Eurasia is assumed to be ~450 km corresponding to 4° of palaeolatitude. Northward convergence first pushed the southern and central Pamirs against the northern Pamirs causing internal shortening of ~170 km (A to B). Then the whole Pamirs moved northward by about 280 km (B to C). In this model convergence within the metamorphic dome and the northern Pamirs is assumed to be negligible.

shortening within the southern (shortened to ~40%) and central (shortened to ~60%) Pamirs.
- Subsequently, the tectonic activities shifted to the northern frontal thrust zone and the whole Pamirs became thrusted over the Alai range.

Acknowledgements

The project was financed by the University of Tübingen and the German Research Council (DFG). Lothar Ratschbacher, Sergei Semiletkin, Sasha Zamouryev, Misha Kornilov, Bernd Greiner, Eberhard Waldhör, Manfred Strecker, Martina Schwab, Peter Blisniuk, Hu Shoyun, Eva Schill, Olaf Zeh, Claudia Bross, Helmut Mayer and many others have been involved with organisation, field work, laboratory measurements, reviews, criticism and discussions.

References

Besse, J., Courtillot, V., 1991. Revised and synthetic apparent polar wander paths of the African, Eurasian, North American and Indian plates, and true polar wander paths since 200 Ma. J. Geophys. Res. 96, 4029–4050.

Burtman, V.S., Molnar, P., 1993. Geological and geophysical evidence for deep subduction of continental crust beneath the Pamir. Spec. Pap. Geol. Soc. Am. 281, 76.

Fisher, R.A., 1953. Dispersion on a sphere. Proc. R. Soc. London, A 217, 295–305.

Kirschvink, J.L., 1980. The least-squares line and plane and the analysis of palaeomagnetic data. Geophys. J. R. Astron. Soc. 62, 699–718.

Klootwijk, C.T., Nazirullah, R., DeJong, K.A., 1986. Palaeomagnetic constraints on formation of the Mianwali reentrant, Trans Indus and Western Salt Range, Pakistan. Earth Planet. Sci. Lett. 80, 394–414.

Klootwijk, C.T., Gee, J.S., Peirce, J.W., Smith, G.M., 1991. Constraints on the India-Asia Convergence: Paleomagnetic Results from Ninetyeast Ridge, in: J. Weissel, J. Peirce, et al. (Eds.), Proc. ODP, Sci. Results, College Station, TX (Ocean Drilling Program), vol. 121, pp. 777–881.

Klootwijk, C.T., Conaghan, P.J., Nazirullah, R., Jong, K.A., 1994. Further palaeomagnetic data from Chitral (Eastern Hindukush): evidence for an early India-Asia contact. Tectonophysics 237, 1–25.

McElhinny, M.W., 1964. Statistical significance of the fold test in palaeomagnetism. Geophys. J. R. Astron. Soc. 8, 338–340.

McFadden, P.L., 1990. A new foldtest for palaeomagnetic studies. Geophy. J. Int. 103, 163–169.

Ogg, J., 1995. Magnetic polarity time scale of the Phanerozoic, in: Ahrens, T. (Ed.) Global Earth Physics: A Handbook of Physical Constants, AGU Reference Shelf series, 1, Am. Geophys. Union, pp. 240–270.

Patzelt, A., Huamei, L., Wang, J., Appel, E., 1996. Palaeomagnetism of Cretaceous to Tertiary sediments from southern Tibet: evidence for the extent of the northern margin of India prior to the collision with Eurasia. Tectonophysics 259, 259–284.

Russian Geology Ministry, 1980. Geological Map of Kyrgyzstan, scale 1:500.000, sheet, J-43-A, St. Petersburg.

Russian Geology Ministry, 1984. Geological Map of the Tadjik SSR and adjoining territories, scale 1:500.000, St. Petersburg.

Schwab, M., Ratschbacher, L., Frisch, W. 1999. Constraining the exhumation history and tectonic evolution of the NE- and Central Pamirs. Terra Nostra, 99(2), 14th Himalaya-Karakoram-Tibet workshop, pp. 138–139.

Strecker, M.R., Frisch, W., Hamburger, M.W., Ratschbacher, L., Semiletkin, S., Zamoruyev, A., Sturchio, N., 1995. Quaternary deformation in the Eastern Pamirs, Tadzhikistan and Kyrgyzstan. Tectonics 14 (5), 1061–1079.

Thomas, J.C., Chauvin, A., Gapais, D., Bazhenov, M.L., Perroud, H., Cobbold, P.R., Burtman, V.S., 1994. Paleomagnetic evidence for Cenozoic block rotations in the Tadjik depression (Central Asia). J. Geophys. Res. 99 (B8), 15 141–15 160.

Waldhör, M., 1999. The small-circle reconstruction in palaeomagnetism and its application to palaeomagnetic data from the Pamirs. Tübinger Geowissenschaftliche Arbeiten, A 45, 99p.